# Constraining the onset of flexural subsidence and peripheral bulge extension in the Miocene foreland of the southern Apennines (Italy) by Sr-isotope stratigraphy

M. Sabbatino [a,*], S. Vitale [a], S. Tavani [a], L. Consorti [b], A. Corradetti [c], A. Cipriani [d,e], I. Arienzo [f], M. Parente [a]

[a] DiSTAR, Università di Napoli Federico II, 21 Via vicinale cupa Cintia, 80126 Napoli, Italy
[b] Department of Mathematics and Geosciences, University of Trieste, 2 Via Weiss, 34124 Trieste, Italy
[c] Department of Petroleum Engineering, Texas A&M University at Qatar, Education City, Doha, Qatar
[d] Department of Chemical and Geological Sciences, University of Modena and Reggio Emilia, 103 Via Campi, 41125 Modena, Italy
[e] Lamont-Doherty Earth Observatory, Columbia University, 61 Route 9W, 10964 Palisades, NY, USA
[f] National Institute of Geophysics and Volcanology, Vesuvius Observatory, 328 Via Diocleziano, 80124 Napoli, Italy

ARTICLE INFO

*Article history:*
Received 22 November 2019
Received in revised form 3 March 2020
Accepted 5 March 2020
Available online 12 March 2020

Editor: Dr. Catherine Chagué

*Keywords:*
Foreland basin system
Forebulge unconformity
Strontium isotope stratigraphy
Forebulge extension
Miocene
Southern Apennines (Italy)

ABSTRACT

In fold and thrust belts developing at convergent margins, the migration of the advancing wedge is accompanied by bulging of the downgoing plate, followed by the development of a foredeep basin filled by a thick succession of syn-orogenic sediments. The transition from forebulge to foredeep marks a key moment in the evolution of the orogenic system. In deep water environments, the record of this transition is typically complete and progressive. Conversely, in the shallow-water/continental environment of many collisional systems, the uplift of the forebulge area can imply emersion and erosion, obliterating the stratigraphic record of key steps of the evolution of the orogenic system. The southern Apennines constitute one of these collisional fold and thrust belts where the development of the forebulge has implied emersion and erosion, with the development of a Miocene forebulge erosional unconformity, accompanied by extensional deformation associated with the bending of the lithosphere during the forebulge stage. In this paper, we use strontium isotope stratigraphy to constrain with unprecedented time-resolution the age of the forebulge unconformity in areas presently incorporated in the northern sector of the southern Apennines fold and thrust belt. Integration of our results and those of previous studies indicates, at the regional scale, a younging toward the foreland of the forebulge unconformity across the belt. Our high-resolution ages also reveal a diachronous onset of the flexural subsidence over short distances, associated with the occurrence of horst and graben structures, possibly resulting from inherited paleotopography along with forebulge extension. This work highlights how high-resolution dating is critical to unravel the evolution of foreland basin systems at different scales.

## 1. Introduction

Foreland basins are key portions of orogenic systems, forming in front and above of thrust belts due to the downward flexing of the lithosphere during convergence (Allen et al., 1986; DeCelles and Giles, 1996). The forebulge is the outermost portion of the thrust belt-foreland basin system, dividing the foreland from the foredeep basin. The bulge consists of a small (generally in the order of less than a few hundreds of meters) and gentle rise of the topography, developing as an elastic response to the flexure of the lithosphere (Turcotte and Schubert, 1982). The first stratigraphic expression of the flexural stage is a regional unconformity between the pre-orogenic sequence and the syn- to post-bulge sediments, commonly referred to as the forebulge unconformity (Crampton and Allen, 1995). The syn-orogenic deposits are wedge-shaped and forelandward thinning, and they are characterized by distinctive time-transgressive sedimentation toward the foreland, as found, for example, in the Carpathians (Leszczyński and Nemec, 2015), Dinarides (Babić and Zupanič, 2008, 2012), Himalayas (DeCelles et al., 1998), Northern Alps (Crampton and Allen, 1995; Sinclair, 1997), Oman-UAE (Glennie et al., 1973; Robertson, 1987; Corradetti et al., 2019), Pyrenees (Vergés et al., 1998), Taiwan (Yu and Chou, 2001), West Interior (White et al., 2002), and Zagros (Alavi, 2004; Saura et al., 2015). The transition from

* Corresponding author.
*E-mail address:* monia.sabbatino@unina.it (M. Sabbatino).

pre-orogenic to syn-orogenic sedimentation in the forebulge area can be either gradual or extremely abrupt, largely depending on the depositional environment of the forebulge area itself (Crampton and Allen, 1995). When bulging occurs in sub-marine environments, the first phase of syn- to post-forebulge sedimentation occurs generally in a deep-water setting, such as in the Aruma Group on Wasia-Aruma Break in Oman-UAE (Robertson, 1987; Boote et al., 1990; Robertson and Searle, 1990; Cooper et al., 2014), and in the Gurpi-Pabdeh Group in Zagros (Vergés et al., 2011; Saura et al., 2015), hence the stratigraphic record associated with the flexural bulge is fully registered. In tectonic settings involving mostly subaerial peripheral bulge areas, distinctive and articulated forebulge unconformities can develop through erosion and karst, such as on top of passive margin rocks of the Adriatic carbonate platform (Otoničar, 2007). Also, subsequent submarine erosion and sediment bypass in shallow-water environments, levelling the bulge unconformity and/or removing condensed forebulge deposits (DeCelles and Giles, 1996), may generate disconformities/paraconformities (White et al., 2002). In view of the above mentioned, in shallow-water/continental environments, the lack of a complete sedimentary record may hinder the full reconstruction of the tectono-sedimentary evolution of the forebulge/foredeep system. In fossil and dismembered foreland basins, the forebulge phase is recorded by the basal portion of the syn-orogenic sedimentary sequence, where time-transgressive unconformities and facies changes track the progressive evolution of the foreland-thrust wedge system (Fig. 1). High-resolution dating of these deposits provides constraints on the main steps of the tectono-sedimentary evolution of the dismembered foreland basin (Sinclair, 1997; Galewsky, 1998; Leszczyński and Nemec, 2015).

A typical example is the Miocene fossil foreland of the southern Apennine belt, which has experienced pre-thrusting bulging, uplift, and erosion, caused by the bending of the subducting lithosphere and the accretionary wedge migration (e.g., Doglioni, 1995), and has been subsequently dismembered and incorporated into the thrust belt during the E/NE-ward migration of the trench (e.g., Roure et al., 1991; Cello and Mazzoli, 1998; Vitale and Ciarcia, 2013; Faccenna et al., 2014). Patches of this foreland basin are now exposed at different localities of the central-southern Apennines. The timing of deformation and the shortening rate of the Apennine fold and thrust belt have been so far reconstructed using the ages of the first siliciclastic deposits of the foredeep and wedge-top basins (e.g., Cipollari and Cosentino, 1995; Bigi et al., 2009; Critelli et al., 2011; Vitale and Ciarcia, 2013). This approach has produced controversial results, since these deposits are poorly fossiliferous and usually dominated by reworked specimens (e.g., De Capoa et al., 2003). An alternative would be to use the age of the Miocene shallow-water carbonate deposits, which represent the base of the foreland basin megasequence, and record the first phase of foreland flexural subsidence during the Apennine thrust sheet belt emplacement. An additional advantage would be that shallow-water carbonates, being more sensitive to sea-level and paleoenvironmental changes compared to deep-water siliciclastics, could give a more detailed record of the first phases of foreland basin evolution (Dorobek, 1995; Galewsky, 1998; Bosence, 2005). However, the Miocene syn-orogenic shallow-water carbonates of the southern Apennines have been so far dated only by biostratigraphy, which is mainly based on miogypsinid larger foraminifera (Schiavinotto, 1979, 1985; Brandano et al., 2007), with limitations imposed by the sparse occurrence of these fossils, and by the low time resolution (not better than 2–4 Ma) and uncertain calibration of larger foraminiferal biozones to the geological time scale (Cahuzac and Poignant, 1997; Hilgen et al., 2012).

In this work, we aim to constrain the sequence of events recording the migration of the southern Apennines fold and thrust belt and of its foreland basin by dating with unprecedented high-resolution the basal levels of the Miocene syn-orogenic shallow-water carbonates. To overcome the above-mentioned limitations of biostratigraphy, we use strontium isotope stratigraphy (McArthur et al., 2012) on the biotic low-Mg calcite of well-preserved bivalve shells, attaining a resolution of 0.1–0.3 Ma.

In addition to the high-resolution dating, we report on joints and sedimentary dykes formed during the Miocene forebulge-related extension. The latter is associated with deformation occurring in the peripheral bulge area, as recognized worldwide in foreland basins (e.g., Tavani et al., 2015a; Martinelli et al., 2019). The timing of syn-orogenic sedimentation in relation to the development of extensional structures provides additional constraints for the reconstruction of the tectono-sedimentary evolution of a foreland basin.

## 2. Geological setting

### 2.1. The Southern Apennines

The southern Apennines are one of the two arcs constituting the Neogene Apennines fold and thrust belt (Fig. 2a). This fold and thrust belt developed due to the W-ward subduction of the Adria plate underneath Europe. The collisional system was characterized by a progressive arching of an originally almost linear belt, due to the E-ward retreat of the trench and the opening of the Tyrrhenian back-arc basin (e.g., Malinverno and Ryan, 1986; Doglioni, 1991; Mazzoli and Helman, 1994; Faccenna et al., 2014). The present-day configuration of the southern Apennines (Fig. 2b) is defined by the tectonic superposition of several thrust sheets, made up of Meso-Cenozoic sediments deposited in basins and carbonate platforms developed on the southern margin of the Alpine Tethys (i.e., in the Adria domain) since the Triassic (Bosellini, 2004). In the study area (Fig. 2b), the top of the tectonic pile is made of units belonging to the Apennine Carbonate Platform, and these units overthrust imbricated thrust sheets made up of deep-water sediments of the Lagonegro-Molise Basin. Before the onset of convergence, this basin was interposed between the Apennine Carbonate Platform to the west and the Apulian Carbonate Platform to the east. The Lagonegro units tectonically cover the Apulian Carbonate Platform, which is buried below the thrust belt and is exposed further to the E/NE, in the foreland region (Fig. 2).

In the Apennine Carbonate Platform, which is the focus of this work, the pre-orogenic passive margin sedimentation was generally in shallow-water conditions and almost continuous from the Middle Triassic to the Late Cretaceous (Zamparelli et al., 1999; Bernoulli, 2001; Simone et al., 2003; Iannace et al., 2007 and references therein), with a long-lasting exposure recorded in some areas by Albian-Cenomanian karst bauxites (Mindszenty et al., 1995; Vitale et al., 2018). Passive margin shallow-water carbonate sedimentation was comparatively less widespread during the Paleogene and it is generally represented by thin and stratigraphically discontinuous deposits (Selli, 1962; Chiocchini et al., 1994). The last phase of shallow-water carbonate sedimentation is recorded during the Miocene by transgressive deposits overlying the Cretaceous or Paleogene substrate (Carannante and Simone, 1996). During the Miocene, the foreland of the central-southern Apennine fold and thrust belt has experienced pre-thrusting bulging, uplift, and erosion caused by the bending of the subducting lithosphere and the migration of the accretionary wedge (e.g., Doglioni, 1995). This tectonic stage is recorded by a regional unconformity, by extensional fracturing and faulting in the uppermost part of the lithosphere, and by the onset of flexural subsidence (e.g., Bradley and Kidd, 1991; Crampton and Allen, 1995; Tavani et al., 2015a). After the last phase of shallow-water carbonate sedimentation in the early Miocene, ongoing flexural subsidence is recorded by drowning of the early Miocene carbonate ramp, recorded by the deposition of hemipelagic marls with planktonic foraminifera (Lirer et al., 2005), followed by deposition of thick sequences of Mio-Pliocene turbiditic calci- and siliciclastic sediments both in foredeep and wedge-top basins (Sgrosso, 1998; Patacca and Scandone, 2007). The foredeep setting is mainly characterized by deposition of siliciclastics derived from the erosion of the orogenic belt and secondarily by volcaniclastic and

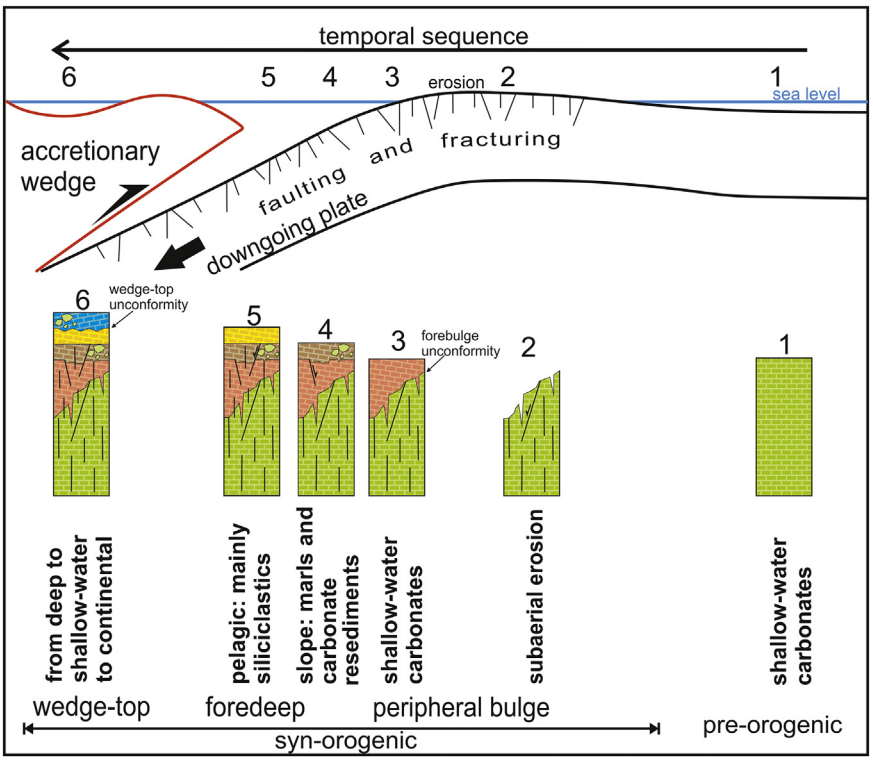


**Fig. 1.** Schematic tectonostratigraphic evolution of a foreland basin system in response to the accretionary wedge migration. The scheme refers to a basin where syn-orogenic sedimentation in the forebulge area starts in shallow-water carbonate system like the Apennine model.

calciclastic sediments. Finally, foredeep deposits are incorporated into the accretionary wedge and overlain by unconformable sediments deposited in wedge-top basins (e.g., Ascione et al., 2012; Vitale and Ciarcia, 2013, 2018). The temporal sequence of the tectonic pulses has been so far constrained by the biostratigraphic ages of the foredeep deposits and of the first unconformable wedge-top basin sediments (Ori et al., 1986; Cipollari and Cosentino, 1995; Bigi et al., 2009; Vitale and Ciarcia, 2013). Fig. 1 shows a cartoon depicting the evolution of the syn-orogenic sedimentation associated with the slab retreat and the accretionary wedge migration.

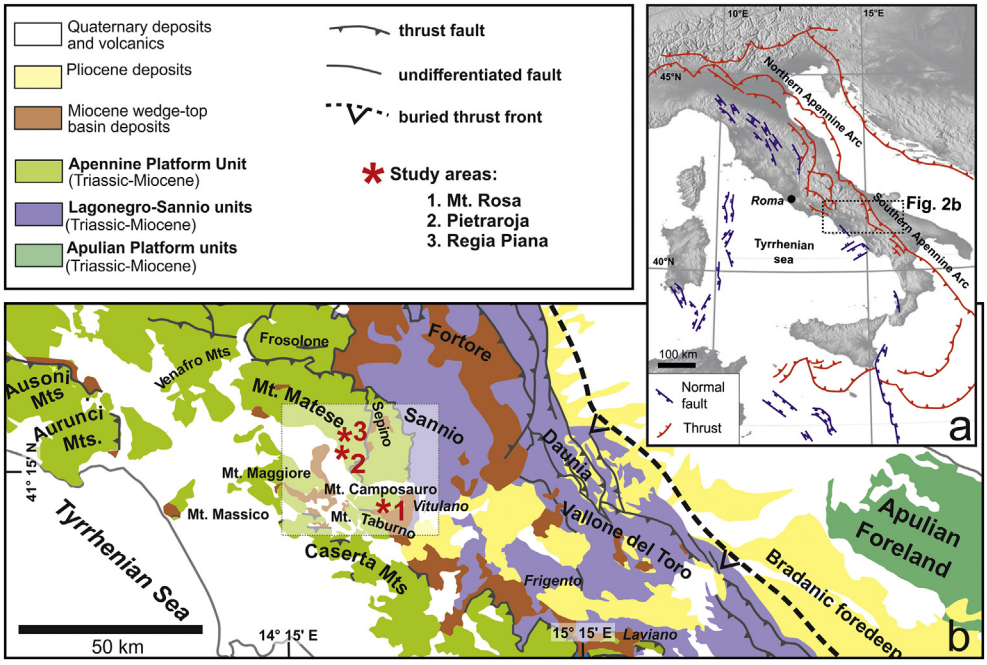


**Fig. 2.** a) Structural scheme of Italy (modified after Tavani et al., 2015b); b) schematic geological map of the northern sector of the southern Apennines showing the locations of the study areas (modified after Vitale and Ciarcia, 2013).

*2.2. Study area*

Our study was performed in the localities of Pietraroja and Regia Piana in the Matese Mountains, and Mount Rosa in the Camposauro Mountain range, in the northern sector of the southern Apennines (Fig. 2b). There, the thick succession (>2000 m) of Upper Triassic to Cretaceous shallow-water carbonate rocks of the Apennine Carbonate Platform is unconformably covered by the red algae and bryozoans limestones of the Burdigalian - Langhian Cusano Formation (Fm.) (Selli, 1957; Carannante and Simone, 1996; Bassi et al., 2010), which pass upward to the hemipelagic Orbulina marls of the Longano Fm. (Selli, 1957), recording the drowning of the platform below the photic zone (Lirer et al., 2005). Above the Longano Fm., the middle Tortonian arenaceous-pelitic turbidites of the Pietraroja Fm. (Selli, 1957) mark the foredeep stage, while the unconformable upper Tortonian–lower Messinian clastic deposits of the Caiazzo Fm. record the wedge-top basin stage (Ogniben, 1958; Vitale et al., 2019).

As mentioned above, the shallow-water limestones of the Cusano Fm. represent the first deposits overlying the regional unconformity that developed during the emersion associated with the forebulge stage (Crampton and Allen, 1995). Together with the Recommone calcarenites, the Roccadaspide and Cerchiara Fms. in the southern Apennines (De Blasio et al., 1981; Carannante et al., 1988a; Carannante and Simone, 1996) and the Briozoi e Litotamni Fm. in the central Apennines (Brandano and Corda, 2002; Civitelli and Brandano, 2005; Brandano et al., 2010), the Cusano Fm. represents the base of the foreland basin mega-sequence of the central-southern Apennines. All these Miocene shallow-water carbonate units are characterized by benthic assemblages dominated by red algae and bryozoans, with variable amounts of larger benthic foraminifers, typical of a temperate-type foramol (*sensu* Lees, 1975) or foramol/rhodalgal carbonate factory (*sensu* Carannante et al., 1988b).

## 3. Material and methods

*3.1. Fieldwork and stratigraphic and structural analysis*

Field observations and sampling, aimed at sedimentological, biostratigraphical and structural analysis, were performed at the three localities (see Fig. 2b). Both the first beds of the Miocene carbonates overlying the forebulge unconformity and the top of the Cretaceous carbonates, just below the unconformity, were studied (see Fig. 3 for a detailed stratigraphy of the studied outcrops). A total of 32 limestone samples were collected, from which 51 thin sections were prepared and studied under an optical microscope, in order to analyze the microfacies, fossil content, diagenetic features and the preservation of the microstructure of the shells or shell fragments to be used for geochemical analyses (Table 1). For the structural study, mesoscale structures were analyzed, such as fractures and sedimentary dykes hosted in both the pre-orogenic Cretaceous carbonates and the syn-orogenic transgressive Miocene limestones. The bedding orientations were also collected, in order to restore all the measured structures to the

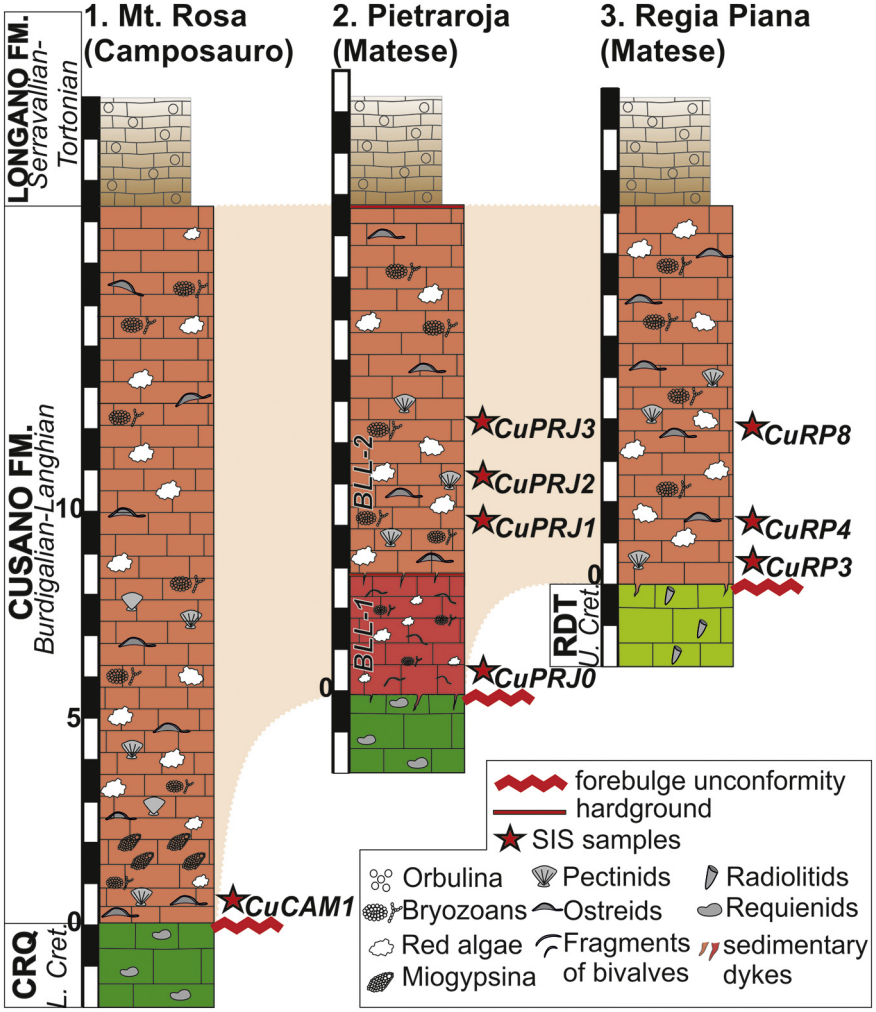


**Fig. 3.** Stratigraphic logs of the studied sections, from left to right: Mt. Rosa (Camposauro Mountain range), Pietraroja and Regia Piana (both in the Matese Mts.).

**Table 1**
Geochemistry of the basal levels of the Cusano Fm. in the studied localities. Pr = preserved, PA = partially altered, A = Altered.

| Sample | Section locality | Latitude | Longitude | m from the base | Material | Mg (ppm) | Sr (ppm) | Fe (ppm) | Mn (ppm) | $^{87}Sr/^{86}Sr$[a] | 2 se ($*10^{-6}$) | Preservation |
|---|---|---|---|---|---|---|---|---|---|---|---|---|
| CuPRJ0a | Pietraroja | 41°20′59″N | 14°33′09″E | 0 | Bivalve shell | 3390 | 445 | 136 | 13 | 0.708516 | 7 | Pr |
| CuPRJ0b | Pietraroja | 41°20′59″N | 14°33′09″E | 0 | Bivalve shell | 3905 | 457 | 127 | 12 | 0.708506 | 7 | Pr |
| CuPRJ0M | Pietraroja | 41°20′59″N | 14°33′09″E | 0 | Matrix bulk | 7381 | 375 | 191 | 21 | 0.708561 | 6 | |
| CuPRJ1a | Pietraroja | 41°20′59″N | 14°33′08″E | 4.5 | Pectinid shell | 2088 | 632 | 82 | 14 | 0.708542 | 8 | Pr |
| CuPRJ1b1 | Pietraroja | 41°20′59″N | 14°33′08″E | 4.5 | Pectinid shell | 2399 | 566 | 148 | 27 | 0.708552 | 6 | Pr |
| CuPRJ1b2 | Pietraroja | 41°20′59″N | 14°33′08″E | 4.5 | Pectinid shell | 2987 | 444 | 77 | 33 | 0.708581 | 8 | PA |
| CuPRJ1c | Pietraroja | 41°20′59″N | 14°33′08″E | 4.5 | Pectinid shell | 2000 | 772 | 63 | 11 | 0.708709 | 5 | A |
| CuPRJ1d | Pietraroja | 41°20′59″N | 14°33′08″E | 4.5 | Pectinid shell | 2947 | 641 | 169 | 22 | 0.708562 | 7 | Pr |
| CuPRJ1M | Pietraroja | 41°20′59″N | 14°33′08″E | 4.5 | Matrix bulk | 3232 | 335 | 99 | 30 | 0.708688 | 6 | |
| CuPRJ2a | Pietraroja | 41°20′59″N | 14°33′06″E | 5 | Pectinid shell | 1886 | 509 | 65 | 33 | 0.708537 | 5 | Pr |
| CuPRJ2b | Pietraroja | 41°20′59″N | 14°33′06″E | 5 | Pectinid shell | 1791 | 492 | 119 | 15 | 0.708541 | 5 | Pr |
| CuPRJ2c | Pietraroja | 41°20′59″N | 14°33′06″E | 5 | Pectinid shell | 1767 | 554 | 87 | 17 | 0.708541 | 5 | Pr |
| CuPRJ2M | Pietraroja | 41°20′59″N | 14°33′06″E | 5 | Matrix bulk | 3111 | 224 | 61 | 38 | 0.708605 | 6 | |
| CuPRJ3a | Pietraroja | 41°21′0″N | 14°33′08″E | 6 | Ostreid shell | 1633 | 437 | 33 | 12 | 0.708712 | 5 | A |
| CuPRJ3b | Pietraroja | 41°21′0″N | 14°33′08″E | 6 | Ostreid shell | 1716 | 409 | 32 | 11 | 0.708704 | 5 | A |
| CuPRJ3c | Pietraroja | 41°21′0″N | 14°33′08″E | 6 | Ostreid shell | 1428 | 578 | 35 | 9 | 0.708506 | 5 | A |
| CuPRJ3M | Pietraroja | 41°21′0″N | 14°33′08″E | 6 | Matrix bulk | 6813 | 376 | 133 | 21 | 0.708556 | 5 | |
| CuRP3b | Regia Piana | 41°21′46″N | 14°32′09″E | 0.2 | Ostreid shell | 948 | 247 | 41 | 14 | 0.708711 | 4 | A |
| CuRP3d | Regia Piana | 41°21′46″N | 14°32′09″E | 0.2 | Ostreid shell | 1455 | 362 | 35 | 9 | 0.708655 | 5 | PA |
| CuRP3e | Regia Piana | 41°21′46″N | 14°32′09″E | 0.2 | Pectinid shell | 2472 | 679 | 49 | 17 | 0.708525 | 8 | Pr |
| CuRP3M | Regia Piana | 41°21′46″N | 14°32′09″E | 0.2 | Matrix bulk | 3103 | 227 | 55 | 18 | 0.708608 | 11 | |
| CuRP4a | Regia Piana | 41°21′46″N | 14°32′09″E | 0.93 | Ostreid shell | 1026 | 222 | 21 | 11 | 0.708682 | 5 | A |
| CuRP4d | Regia Piana | 41°21′46″N | 14°32′09″E | 0.93 | Ostreid shell | 1543 | 389 | 57 | 11 | 0.708661 | 7 | PA |
| CuRP4M | Regia Piana | 41°21′46″N | 14°32′09″E | 0.93 | Matrix bulk | 3958 | 309 | 77 | 19 | 0.708620 | 11 | |
| CuRP8a | Regia Piana | 41°21′46″N | 14°32′09″E | 2 | Ostreid shell | 2500 | 560 | 60 | 12 | 0.708692 | 12 | PA |
| CuRP8b | Regia Piana | 41°21′46″N | 14°32′09″E | 2 | Pectinid shell | 769 | 362 | 36 | 9 | 0.708510 | 5 | PA |
| CuRP8c | Regia Piana | 41°21′46″N | 14°32′09″E | 2 | Ostreid shell | 1607 | 1060 | 36 | 12 | 0.708503 | 11 | PA |
| CuRP8d | Regia Piana | 41°21′46″N | 14°32′09″E | 2 | Ostreid shell | 2314 | 571 | 231 | 5 | 0.708658 | 8 | PA |
| CuRP8M | Regia Piana | 41°21′46″N | 14°32′09″E | 2 | Matrix bulk | 3626 | 297 | 88 | 22 | 0.708543 | 6 | |
| CuCAM1a | Mt. Rosa | 41°10′32.53″N | 14°34′41.14″E | 0.5 | Ostreid shell | 1975 | 998 | 9 | 4 | 0.708713 | 8 | Pr |
| CuCAM1b | Mt. Rosa | 41°10′32.53″N | 14°34′41.14″E | 0.5 | Pectinid shell | 2011 | 670 | 188 | 11 | 0.708690 | 7 | Pr |
| CuCAM1b4 | Mt. Rosa | 41°10′32.53″N | 14°34′41.14″E | 0.5 | Ostreid shell | 1939 | 527 | 24 | 7 | 0.708737 | 6 | PA |
| CuCAM1c | Mt. Rosa | 41°10′32.53″N | 14°34′41.14″E | 0.5 | Ostreid shell | 2164 | 482 | 66 | 11 | 0.708735 | 6 | PA |
| CuCAM1e | Mt. Rosa | 41°10′32.53″N | 14°34′41.14″E | 0.5 | Ostreid shell | 2236 | 489 | 6 | 8 | 0.708729 | 6 | PA |
| CuCAM1f | Mt. Rosa | 41°10′32.53″N | 14°34′41.14″E | 0.5 | Pectinid shell | 1847 | 745 | 6 | 8 | 0.708715 | 6 | Pr |
| CuCAM1g | Mt. Rosa | 41°10′32.53″N | 14°34′41.14″E | 0.5 | Ostreid shell | 2519 | 529 | 2 | 7 | 0.708706 | 10 | Pr |
| CuCAM1M | Mt. Rosa | 41°10′32.53″N | 14°34′41.14″E | 0.5 | Matrix bulk | 4556 | 312 | 123 | 13 | 0.708704 | 6 | |

[a] Sr isotope ratios measured in the lab have been corrected for interlaboratory bias; see Section 3 of the text for further explanations.

horizontal. During the data collection, particular attention was paid to the abutting and cross-cutting relationships. The analysis of these mesoscale structures was aimed at reconstructing the stress field orientation at the time of the unconformity development, to check its consistency with deformation expected in the forebulge area.

### 3.2. Strontium isotope stratigraphy

Strontium isotope stratigraphy (SIS) is based on the empirical observation that the Sr-isotope ratio ($^{87}Sr/^{86}Sr$) of the ocean has varied through time, and on the assumption (verified in the modern ocean and consistent with the long residence time of Sr) that, at any moment in the geological past, the Sr-isotope ratio of the ocean was homogeneous (DePaolo and Ingram, 1985; McArthur, 1994). A reference curve documenting the $^{87}Sr/^{86}Sr$ value of the ocean through geological time, has been assembled by means of well-dated and diagenetically pristine samples of marine precipitates (McArthur et al., 2001) and has been continuously refined and calibrated to the most recent geological time scale (McArthur et al., 2012). SIS is particularly suitable for high-resolution dating and correlation of Miocene marine carbonates because the reference curve for this stratigraphic interval is characterized by a very narrow statistical uncertainty and by a very high slope (i.e., rapid unidirectional change of $^{87}Sr/^{86}Sr$ ratio of the ocean through time). For these reasons, a resolution of 0.1 Ma can be potentially attained in Miocene marine deposits. A prerequisite for successful application of SIS is to select unaltered marine precipitates that have retained their pristine Sr isotope ratio. Biotic low-Mg calcite is a suitable material, because it is more resistant to diagenetic alteration and because its degree of diagenetic alteration can be checked with a suite of petrographic and geochemical analyses (McArthur, 1994; Ullmann and Korte, 2015). In Miocene shallow-water carbonate units of the Apennines, this material is provided in pectinid and ostreid bivalves.

The dataset used for SIS consists of 43 sub-samples, derived from 27 limestone samples containing shells or fragments of ostreids and pectinids collected from the base of Cusano Fm. (see Table 1 and Fig. 3 for details about locality, geographic coordinates, stratigraphic position, and type of material).

The preservation of the original microstructure of the bivalve shells was assessed by petrographic observation with a standard optical microscope and with a scanning electron microscope (SEM). Based on these observations, the state of preservation was recorded as "preserved" (Pr) or "altered" (A). The notation "partially altered" (PA) was used for shells that showed moderately well-preserved portions side by side with altered portions (Table 1).

In order to get a more complete understanding of the impact of diagenesis on the different components of the studied samples, all the shells, including the petrographically altered ones, and the matrix enclosing the shells, were measured for the concentration of minor and trace elements and for the Sr isotope ratio. About 8–10 mg of calcite powder was obtained from each subsample by careful microdrilling with a tungsten bit under an optical microscope. Concentrations of Mg, Sr, Fe, and Mn (Table 1) were determined through inductively coupled plasma optical emission spectroscopy (ICP-OES) - UNICAM PU 7000 at the Institut für Geologie, Mineralogie und Geophysik of the Ruhr-Universität of Bochum (Germany) for some samples and by using an ICP-OES Perkin Elmer Optima 4200 DV at the Department of

Chemistry and Earth Science of the University of Modena and Reggio Emilia (Italy), for the remaining set of samples.

Strontium isotope ratios were measured in three different laboratories. The first batch of samples was analyzed using a thermal-ionization mass spectrometer (TIMS) Finnigan MAT 262 at the Institut für Geologie, Mineralogie und Geophysik of the Ruhr-Universität of Bochum. The second one was analyzed by means of a high-resolution multi-collector inductively coupled plasma mass spectrometer (MC-ICP-MS) Thermo Scientific Neptune, at the Centro Interdipartimentale Grandi Strumenti (CIGS) of the University of Modena and Reggio Emilia. The third group of samples was analyzed with a ThermoFinnigan Triton multi-collector TIMS at the National Institute of Geophysics and Volcanology, Vesuvius Observatory in Naples (Italy). All geochemical data are given in Table 1, while details on sample preparation, analytical procedures, precision and reproducibility of the analyses and the values of the laboratory standards are given in the supplementary material. The $^{87}Sr/^{86}Sr$ values measured in the labs are considered to be free of inter-laboratory bias since, during the collection of isotopic data, replicate analyses of the standards were performed to check for external reproducibility. Sr isotope ratios were normalized to the value of the NIST–SRM 987 standard used by McArthur et al. (2001) for their compilation.

Only the Sr isotope ratios of the shells that are considered to have retained their pristine Sr isotope value were used for SIS. The diagenetic screening process followed the multistep procedure outlined in Frijia and Parente (2008) and Frijia et al. (2015), incorporating i. petrographic observation of the shell microstructure, ii. sample by sample evaluation of the geochemical composition of the different components (well-preserved shells, altered shells and bulk matrix), and iii. internal consistency of the Sr isotope ratios of different shells from the same stratigraphic level.

Numerical ages were derived from the Sr isotope ratios by means of the look-up table of McArthur et al. (2001; version 5: 03/13). When more than one shell was available for the same stratigraphic level, the SIS age was derived from the mean value calculated from all the shells. Minimum and maximum ages were obtained by combining the statistical uncertainty of the samples, given by 2 standard error (2 s.e.; McArthur, 1994) of the mean value, with the uncertainty of the reference curve (see Steuber, 2003, for an explanation of the method). When less than four shells per level were analyzed, the precision of the mean value was considered to be not better than the average precision of single measurements, given as 2 s.e. of the mean value of the standards. The numerical ages obtained from the look-up table were translated into chronostratigraphic ages by reference to the Geological Time Scale of Gradstein et al. (2012) (hereinafter GTS2012), to which the look-up table is tied.

## 4. Results

### 4.1. Stratigraphy and facies

In the study area, the regional forebulge unconformity between the syn-orogenic lower Miocene shallow-water carbonates and the pre-orogenic substrate is represented by a paraconformity or a disconformity at the scale of the outcrop (Fig. 4a, c). The unconformity surface is generally marked by pressure solution structures such as stylolites (Figs. 5a, 6a). At the top of the Cretaceous substrate, breccia levels, sometimes accompanied by red crusts, are reported in some localities of the Mt. Camposauro area (Carannante et al., 2013). The uppermost levels of the Cretaceous substrate range in age from the Early Cretaceous (i.e., Aptian at Pietraroja and Mt. Rosa sections) to the Late Cretaceous (i.e., Coniacian at Regia Piana) (Simone et al., 2003; Carannante et al., 2013).

At Pietraroja, the Miocene carbonates of the Cusano Fm. cover a Lower Cretaceous substrate, which can be dated as Aptian due to the presence of the foraminifers *Sabaudia capitata* Arnaud-Vanneau, *Sabaudia minuta* (Hofker), *Cuneolina laurentii* (Sartoni and Crescenti) and *Nezzazata isabellae* Arnaud-Vanneau and Sliter (Chiocchini et al., 1994). The first Miocene level in the Pietraroja section (BLL-1 lithofacies in Bassi et al., 2010), is composed of about 4–5 m of bryozoan and rhodolith floatstone with a fine-grained matrix containing serpulids, echinoid fragments and spines, thin-shelled bivalves, benthic

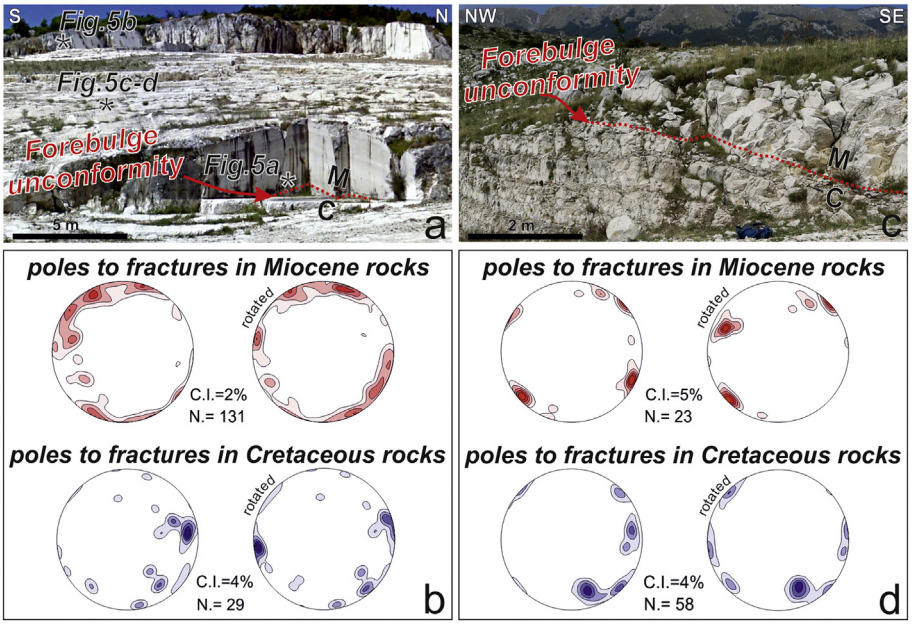


**Fig. 4.** a) Pietraroja section, well-exposed in an abandoned quarry. Forebulge unconformity between the lower Miocene Cusano Fm. (M) and the Lower Cretaceous (Aptian) Calcari a Requienie Fm. (C). The black stars indicate the location of Fig. 5a, c, d. b) Contouring of poles to fractures analyzed at the Pietraroja site at the top of the Cretaceous substrate and within the Miocene carbonates (in blue and red, respectively), in their present-day configuration and after bedding-dip removal. c) Forebulge unconformity at the Regia Piana between the Upper Cretaceous Calcari a Radiolitidi Fm. (C) and the lower Miocene Cusano Fm. (M). d) Contour plots of poles to fractures analyzed at Regia Piana at the top of the Cretaceous substrate and within the Miocene carbonates (in blue and red, respectively), in their present-day configuration and after bedding-dip removal. C.I.: contour increment; N.: data number.

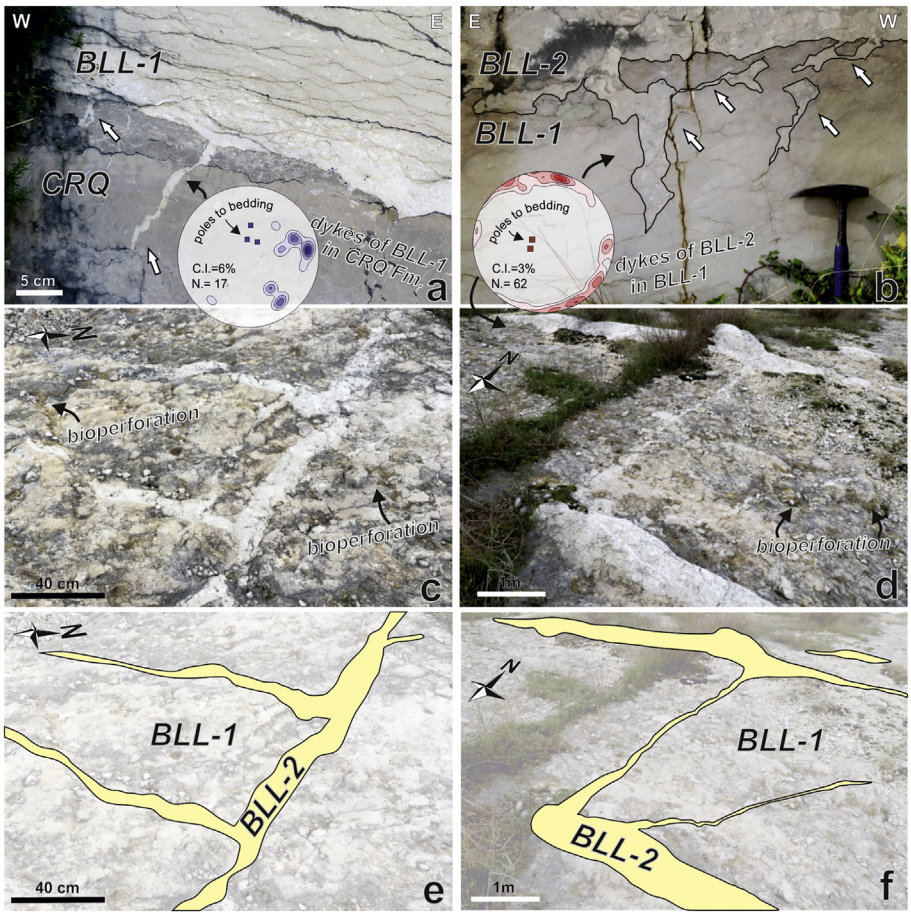


**Fig. 5.** a) Detail of two sedimentary dykes (white arrows) cutting the Calcari a Requienie Fm. (CRQ) of Pietraroja site, filled by the first Miocene deposits (BBL-1) of the Cusano Fm. b) Contact between the rhodolith float-rudstones, facies BLL-2 (above), and the bryozoan-rhodolith floatstones, BLL-1 (below), of the Cusano Fm in the Pietraroja site. These two lithofacies are separated by a hardground (pinkish level). White arrows indicate sedimentary dykes filled by BLL-2 sediments in BBL-1 bedrock, oriented almost N-S and subordinately E-W. c, d) Sedimentary dykes in the basal lithofacies (BLL-1) of Cusano Fm., filled by sediments of the overlying lithofacies (BLL-2). e, f) Line-drawing of the sedimentary dykes showing the predominant E-W and N-S orientations. Contour plots indicate poles to planes of dykes hosted on top of pre-orogenic carbonates (CRQ, blue-colored) and in basal levels of syn-orogenic carbonates (BLL-1, red-colored). The blue and red squares represent the poles to bedding planes of Cretaceous and Miocene carbonates, respectively.

foraminifers (including *Heterostegina* sp., *Amphistegina* sp., *Operculina* sp. and *Sphaerogypsina* sp.) and few planktonic foraminifers (Fig. 6b). This interval is truncated upward by a submarine hardground with evidence of intense bioperforation (Fig. 5c, d) (Bassi et al., 2010). Above the hardground, sedimentation resumed with deposition of bryozoan and rhodolith floatstone to rudstone with a coarser-grained matrix (Figs. 5b–f, 6c, d) (BLL-2 lithofacies in Bassi et al., 2010), containing ostreids, pectinids, echinoid fragments and spines, benthic foraminifers (including *Amphistegina* sp., *Sphaerogypsina* sp. and small rotaliids), some planktonic foraminifers and also re-sedimented clasts of the underlying BLL-1 lithofacies.

In the Regia Piana section, the contact between the Miocene limestones and the Upper Cretaceous substrate, dated as Coniacian due to the occurrence of the foraminifers *Accordiella conica* Farinacci, *Dicyclina schlumbergeri* Munier-Chalmas, *Moncharmontia apenninica* (De Castro) and *Rotalispira scarsellai* (Torre) (Chiocchini et al., 1994), is marked by a stylolitic surface (Figs. 4c, 6a) and is usually densely bored by lithophagous organisms (Fig. 6a). The basal interval of the Cusano Fm. consists of a rhodolith floatstone with bryozoans, ostreids, pectinids, echinoid fragments and spines, benthic foraminifers (such as *Amphistegina* sp., *Sphaerogypsina* sp., and rotaliids), and few planktonic foraminifers (Fig. 6a).

In the Mt. Camposauro area, the Cusano Fm. overlies a Lower Cretaceous substrate, which can be dated as upper Aptian due to the presence of *Archaeoalveolina reicheli* (De Castro) and *Cuneolina laurentii* (Sartoni and Crescenti). In the studied outcrop, the contact is sharp and marked by a stylolitic surface. The basal lower Miocene deposits consist of rhodolith rudstone to floatstone, with subordinated bryozoans, ostreids, pectinids, echinoid fragments and spines, and benthic foraminifers (*Amphistegina* sp. and some rotalids) (Fig. 6e). *Miogypsina intermedia* Drooger was reported by Schiavinotto (1985) in a level about 1 m above the base of the Cusano Fm.

### 4.2. Strontium isotope stratigraphy

#### 4.2.1. Pietraroja

The dataset for the locality of Pietraroja consists of four samples from four different stratigraphic levels (Table 1; Figs. 3, 7c–e). The lowest one (CuPRJ0) was taken very close to the base of the Cusano Fm., within the unit labelled BLL1 by Bassi et al. (2010). The other three come from unit BLL2, which is separated from BLL1 by a bioeroded hardground (Fig. 3).

The Sr concentration of the two shell fragments of undetermined bivalves of sample CuPRJ0 (445–457 ppm) is below the 600 ppm threshold value proposed by Scasso et al. (2001) for well-preserved Miocene pectinids. However, the microstructure of these two shell fragments is well preserved, with no evidence of diagenetic recrystallization. Moreover, the Sr isotope ratio of the two shell fragments is almost within analytical error while it is significantly different from the value of the bulk

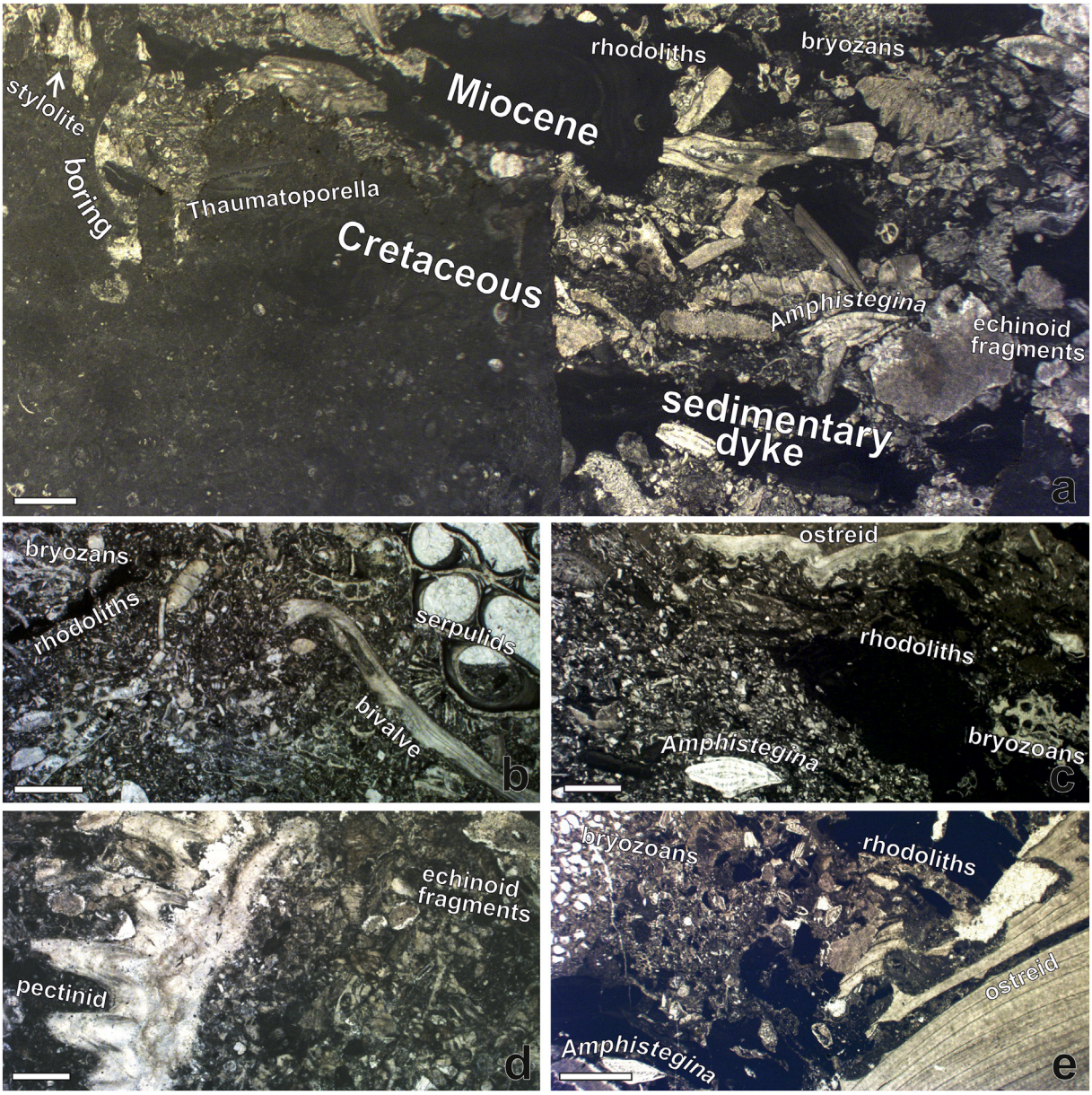


**Fig. 6.** Microfacies of the lower Miocene (Burdigalian) Cusano Fm. in the studied sections. a) Detail of the stylolitic contact between the Cusano Fm. and the Upper Cretaceous pre-orogenic carbonates at Regia Piana. The lower Miocene sediments fill borings and sedimentary dykes in the Cretaceous substrate. The basal levels of the Cusano Fm. are a rhodolith floatstone. b) The lithofacies BLL-1 (Bassi et al., 2010) at Pietraroja is a bryozoan and rhodolith floatstone with a fine-grained matrix. c) Above the hardground at Pietraroja, the BLL-2 facies is characterized by a bryozoan and rhodolith rudstone to floatstone with a coarser-grained matrix. d) Rudstone of the Cusano Fm, about 2 m above the hardground. e) The basal deposits of the Cusano Fm. at Mt. Camposauro are a rhodolith rudstone to floatstone. See the text for more detailed descriptions. Scale bar = 1 mm in all photographs.

matrix enclosing the shells (Fig. 8a). For these reasons, we consider that the $^{87}Sr/^{86}Sr$ value of the shells has not been significantly altered by diagenesis. The mean value of the Sr isotope ratio calculated for CuPRJ0 gives an age of 18.7 Ma (Table 2).

Of the five shells fragments obtained from sample CuPRJ1 (Fig. 7c), CuPRJ1c was discarded, because of petrographic evidence of recrystallization. Its Sr isotope ratio has most probably been significantly altered by diagenesis, as it differs significantly from the values obtained from the other shells of the same sample, while it is very similar to the value obtained from the bulk matrix (Table 2, Fig. 8a). CuPRJ1b2 shows minor evidence of recrystallization. Moreover, its Sr concentration and Sr isotope ratio plot halfway between the well-preserved shells and the bulk matrix (Fig. 8a). For these reasons, this shell was considered as partially altered and was not used for SIS.

The three pectinid shells of sample CuPRJ2 are well preserved, with no petrographic evidence of recrystallization (Fig. 7d). Their Sr isotope ratios are analytically indistinguishable, while they are significantly different from the values obtained from the bulk matrix enclosing the shells (Table 2, Fig. 8a). For all these reasons, their $^{87}Sr/^{86}Sr$ values are considered as pristine (i.e. not altered by diagenesis). The stratigraphic distance between samples CuPRJ1 and CuPRJ2 is just 0.5 m and there is no sedimentological evidence of stratigraphic breaks between them. Therefore, as the Sr isotope values of the well-preserved shells of these samples define a very narrow range (0.708537–0.708562), they have been lumped together for SIS. The mean $^{87}Sr/^{86}Sr$ value calculated for CuPRJ1-CuPRJ2, after excluding the altered shells, is 0.708546, corresponding to a numerical age of 18.3 Ma (Table 2).

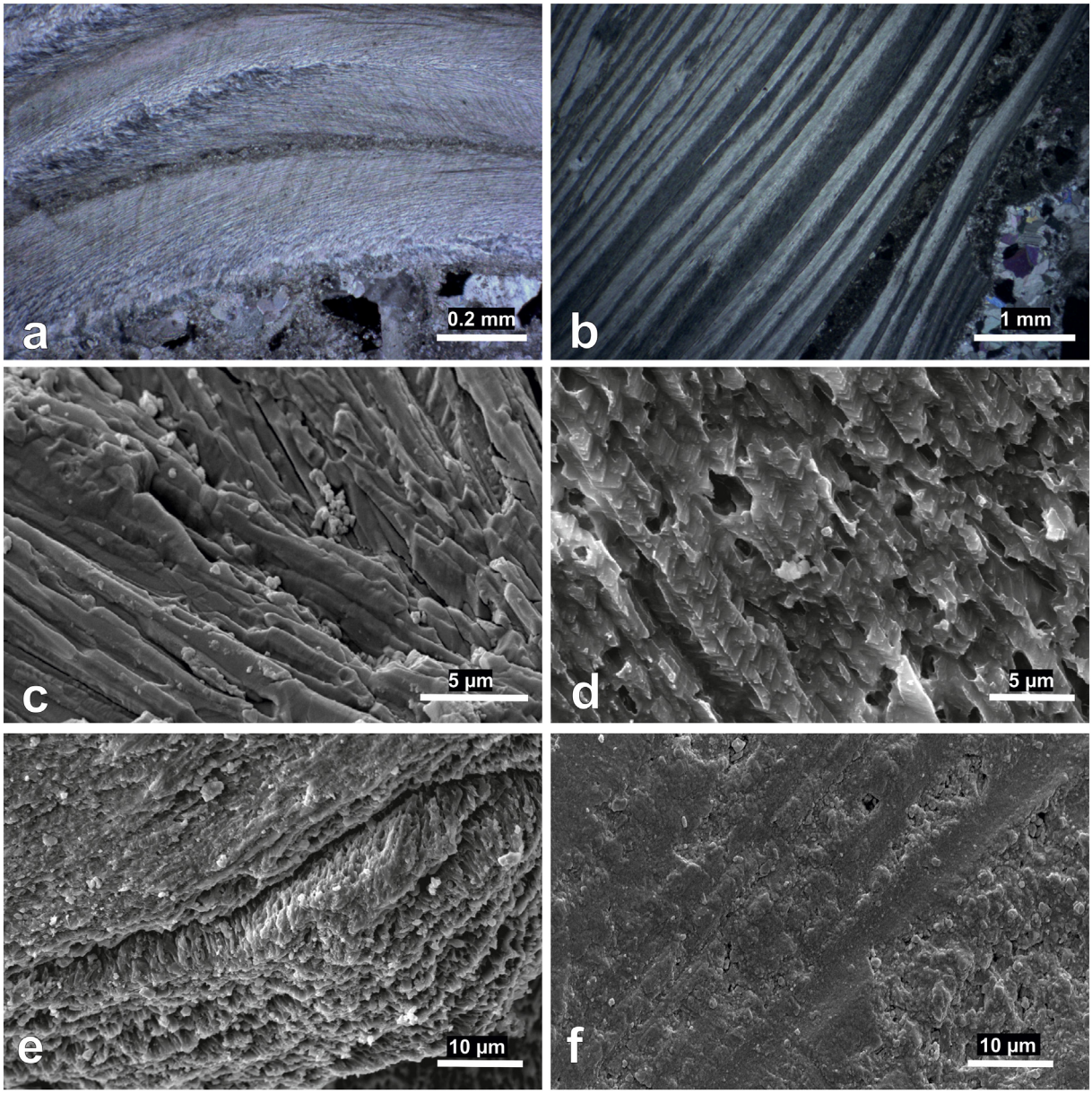


**Fig. 7.** Microphotographs of Miocene pectinid and ostreid shells under optical and scanning electron microscopy. a, b) Ostreid shells at crossed nicols: in a) sample CuRP8c shows parts in which the lamellar microstructure is well-preserved; in b) sample CUCAM1a has a perfectly pristine lamellar microstructure. c, d) Pectinid shells of samples CuPRJ2b and CuPRJ1b1, showing well-preserved lamellar and cross-lamellar ultrastructure with single well-recognizable calcite fibers. e, f) Ostreid shells of samples CuPRJ3b and CuRP3b, showing different alteration degrees: in e) the original lamellar microstructure is still visible, but it has been altered by diagenesis, while in f) the microstructure has been almost completely obliterated by recrystallization.

The three ostreid shell fragments of sample CuPRJ3 show petrographic evidence of recrystallization (Fig. 7e). Moreover, their Sr isotope ratios are very discordant (0.708506–0.708712) (Fig. 8a). For these reasons, they are considered to have been significantly altered by diagenesis and were not used for SIS.

*4.2.2. Regia Piana*

The dataset for the locality Regia Piana consists of three samples from three different stratigraphic levels, within two meters stratigraphic distance from the base of the Cusano Fm. (Fig. 3). The three shell fragments of sample CuRP3, give very discordant Sr isotope ratios (0.708525–0.708711). The two ostreid shells show evidence of recrystallization and have very low Sr concentrations, similar to that of the enclosing matrix (Table 1, Fig. 8b). Their Sr isotope ratios are significantly higher than that of the pectinid shell (CuRP3e), which has a well-preserved microstructure and a Sr concentration falling within the range of well-preserved Miocene pectinids defined by Scasso et al. (2001). For these reasons, only CuRP3e was used for SIS (Fig. 8b). Its $^{87}Sr/^{86}Sr$ value corresponds to a numerical age of 18.6 Ma (Table 2).

All the shell fragments of samples CuRP4 and CuRP8, mostly consisting of ostreids, notwithstanding preserved areas (Fig. 7a), show petrographic and geochemical evidence of diagenetic alteration and were not used for SIS (Table 1, Fig. 8b).

*4.2.3. Mt. Camposauro*

The dataset for the Mt. Camposauro area consists of seven shell fragments (two pectinids and five ostreids) coming from a single stratigraphic level 0.5 m above the base of the Cusano Fm. (Fig. 3). On a plot of Sr concentration vs Sr isotope ratio, the shell fragments define two separate clusters (Fig. 8c). One cluster is made by three shell

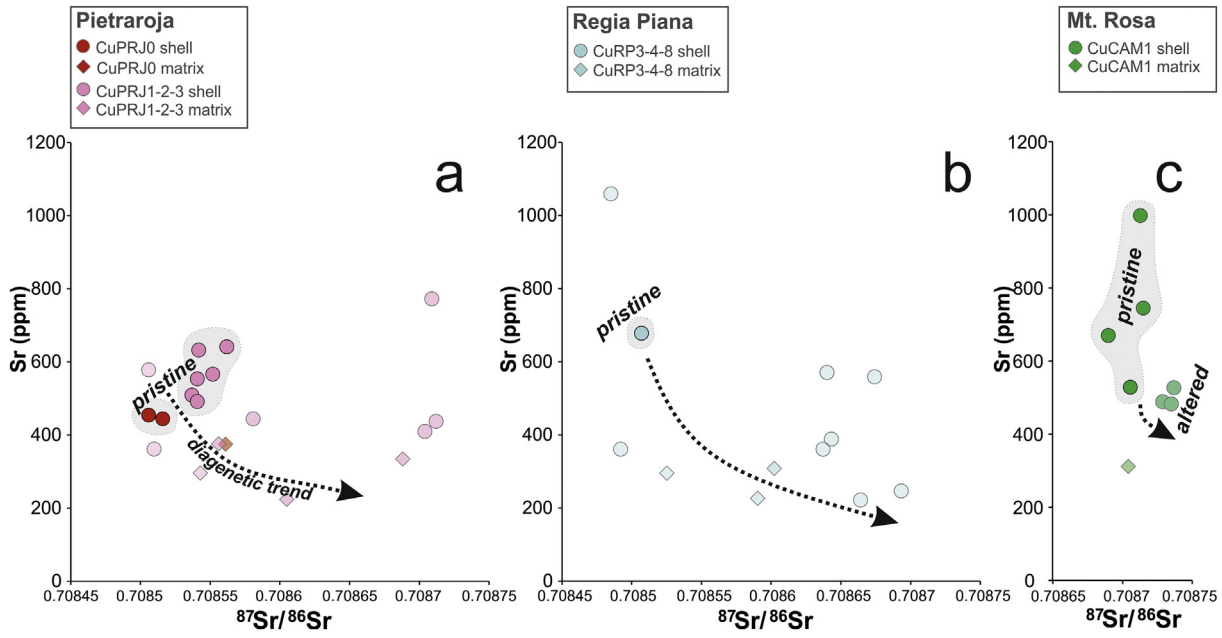


**Fig. 8.** Bivariate scatterplot of Sr concentration vs $^{87}Sr/^{86}Sr$ ratio of the analyzed samples a) at Pietraroja, b) Regia Piana, and c) Camposauro sites.

fragments of ostreids, characterized by petrographic evidence of recrystallization and by higher Sr isotope ratios (0.708729–0.708737) with lower Sr concentration (482-527 ppm) (Fig. 8c). The other cluster consists of four shell fragments (two pectinids and two ostreids) with well-preserved microstructure (Fig. 7b), lower Sr isotope ratios (0.708690–0.708715) and higher Sr concentrations (539–998 ppm). These four shell fragments are considered to have retained their pristine Sr isotope ratios and were used for SIS (Fig. 8c). Their mean $^{87}Sr/^{86}Sr$ value corresponds to a numerical age of 16.3 Ma (Table 2).

### 4.3. Fracture pattern analysis

The structural analysis, performed on both the pre-orogenic carbonate megasequence and the basal part of the syn-orogenic carbonates, shows the occurrence of a fracture network mostly made of two sets, oriented orthogonal to each other and nearly perpendicular to bedding. A total of >300 meso-structural data, including bedding surfaces, joints, veins, and sedimentary dykes, were collected at Pietraroja and Regia Piana sites (Figs. 4, 5). In different outcrops, joints, veins, and sedimentary dykes display the same orientation, suggesting a common extensional origin. Accordingly, these structures are grouped together in the plots of Fig. 4, and they are termed "fractures". Fracture orientation data are displayed in their present-day orientation and in the unfolded state (i.e., removing the bedding dip), in order to better visualize the pre-folding fracture sets (Tavani et al., 2018). The difference between the present-day and unfolded analysis is minimal, due to the very gently dips which characterize the bedding surfaces. The fractures measured on top of the Cretaceous substrate at the Pietraroja site are characterized by poles forming two clusters corresponding to bedding-perpendicular fractures striking N-S and, subordinately, E-W (contour plot in blue, Fig. 4b). In the same section, poles to fractures, hosted in the Miocene limestones, are clustered in three sets, corresponding to bedding perpendicular surfaces striking E-W, N-S, and NE-SW (contour plot in red, Fig. 4b). Fig. 5a shows in detail sedimentary dykes cutting the Cretaceous bedrock in the Pietraroja site (CRQ, Calcari a Requienie Fm.) and filled by the first sediments of the Cusano Fm. (BLL-1). Data on sedimentary dykes collected in this portion of the multilayer are shown in Fig. 5b–f, with their contour plots in the present-

**Table 2**
Strontium isotope stratigraphy of basal levels of the Cusano Fm. in the studied localities.

| Sample | Section locality | m from the base | $^{87}Sr/^{86}Sr$[a] | 2 se ($*10^{-6}$) | $^{87}Sr/^{86}Sr$ mean | 2 se ($*10^{-6}$) | Numerical age (Ma)[b] | | |
|---|---|---|---|---|---|---|---|---|---|
| | | | | | | | Min | Mean | Max |
| CuPRJ0a | Pietraroja | 0 | 0.708516 | 7 | 0.708511 | 10 | 18.5 | 18.7 | 18.9 |
| CuPRJ0b | | 0 | 0.708506 | 7 | | | | | |
| CuPRJ1a | | 4.5 | 0.708542 | 8 | 0.708546 | 8 | 18.2 | 18.3 | 18.5 |
| CuPRJ1b1 | | 4.5 | 0.708552 | 7 | | | | | |
| CuPRJ1d | | 4.5 | 0.708562 | 5 | | | | | |
| CuPRJ2a | | 5 | 0.708537 | 5 | | | | | |
| CuPRJ2b | | 5 | 0.708541 | 5 | | | | | |
| CuPRJ2c | | 5 | 0.708541 | 5 | | | | | |
| CuRP3e | Regia Piana | 0.2 | 0.708525 | 8 | 0.708525 | 15 | 18.4 | 18.6 | 18.9 |
| CuCAM1a | Mt. Rosa | 0.5 | 0.708713 | 8 | 0.708706 | 11 | 16 | 16.3 | 16.5 |
| CuCAM1b | | 0.5 | 0.708690 | 7 | | | | | |
| CuCAM1f | | 0.5 | 0.708715 | 6 | | | | | |
| CuCAM1g | | 0.5 | 0.708706 | 10 | | | | | |

[a] Sr isotope ratios measured in the lab have been corrected for interlaboratory bias; see Section 3 of the text for further explanations.
[b] The preferred numerical age has been derived from the look-up table of McArthur et al. (2001; version 5: 04/13). The minimum and max age are calculated by combining the statistical uncertainty of the samples (2 se of the mean) with the uncertainty of the reference curve (see the methods section in Frijia et al., 2015, for a detailed explanation of the procedure).

day orientation showing the same clustering as those of Fig. 4b, i.e. dykes are bedding-perpendicular and striking N-S and E-W. These dykes, appearing only on top of the BLL-1 interval of the Cusano Fm. (Bassi et al., 2010), are the result of sedimentary infilling of open fractures by sediments of the lithofacies BLL-2 of the Cusano Fm. (Bassi et al., 2010).

At the Regia Piana section, fractures collected in Cretaceous rocks (RDT - Calcari a Radiolitidi Fm.) underlying the forebulge unconformity, define two mutually orthogonal sets of bedding perpendicular surfaces, striking nearly NNW-SSE and WSW-ENE (Fig. 4d). The orientation of fractures measured in the Miocene rocks is quite similar. These fractures, indeed, are bedding-perpendicular and oriented NE-SW and NW-SE (Fig. 4d).

## 5. Discussion

The SIS data presented in this paper supply for the first-time precise constraints on the age of the first lower Miocene deposits overlying the forebulge unconformity in the northern sector of the southern Apennines. The age for the base of the syn-orogenic sequence is rather diachronous, varying from 18.7 Ma at Pietraroja, 18.6 Ma at Regiapiana to 16.3 Ma in the Mt. Camposauro area.

The forelandward migration of a foreland basin system can be constrained by dating the first syn-orogenic deposits overlying the forebulge unconformity (DeCelles and Giles, 1996; DeCelles, 2012). Such migration is driven by the interplay of the load of the orogenic wedge, the load of the downgoing plate and the trench retreat, which define the tectonic setting. The latter also delineates the architecture, sedimentology and structure of the foreland basins (DeCelles, 2012). Accordingly, three main types of contractional foreland basin settings can be defined: retroarc, collisional, and collisional with retreating subducting slabs (DeCelles 2012, pp. 411–416, for a detailed review). In these settings, four depozones are generally observed: wedge-top, foredeep, forebulge and back-bulge (DeCelles and Giles, 1996). The Apennines represent a typical example of a retreating collisional belt, characterized by narrow but thick foredeep and wedge-top depozones, and very narrow forebulge and back-bulge depozones (DeCelles, 2012). The vertical "Waltherian sequence" of foreland basin depozones (DeCelles, 2012) for the Apennine foreland basin is represented by the basal subaerial forebulge unconformity overlain by three diachronous lithostratigraphic units (Fig. 9). From bottom to top these are: (i) a shallow-water carbonate unit, (ii) a hemipelagic marl unit overlain by (iii) a siliciclastic turbidite unit ("underfilled trinity"; Sinclair, 1997).

The rate of migration of the southern Apennine foreland basin-belt system and the amount of shortening are highly debated (e.g., Dewey et al., 1989; Faccenna et al., 2001; Vitale and Ciarcia, 2013) with stratigraphic constraints derived exclusively from the deposits of the wedge-top and foredeep depozones (Cosentino et al., 2010; Vitale and Ciarcia, 2013 and references therein). However, the siliciclastic turbidite deposits of foredeep and wedge-top depozones are characterized by poorly fossiliferous micro- and nannofossil assemblages generally dominated by reworked taxa (De Capoa et al., 2003), which have resulted in uncertain and controversial biostratigraphic dating (e.g., Bonardi et al., 1985; Baruffini et al., 2000; Noguera and Rea, 2000). On the other hand, the deposits of the forebulge and back-bulge depozones have been poorly investigated, leaving a gap in the knowledge of the first steps of the foreland basin evolution. The first shallow-water sediments overlying the forebulge unconformity are generally represented in the study area by middle ramp deposits. These deposits do not record the first marine ingression, because above the fair-weather wave-base the platform was shaved by wave and currents (Brandano, 2017) and sediments did not accumulate. Therefore, the first marine sediments

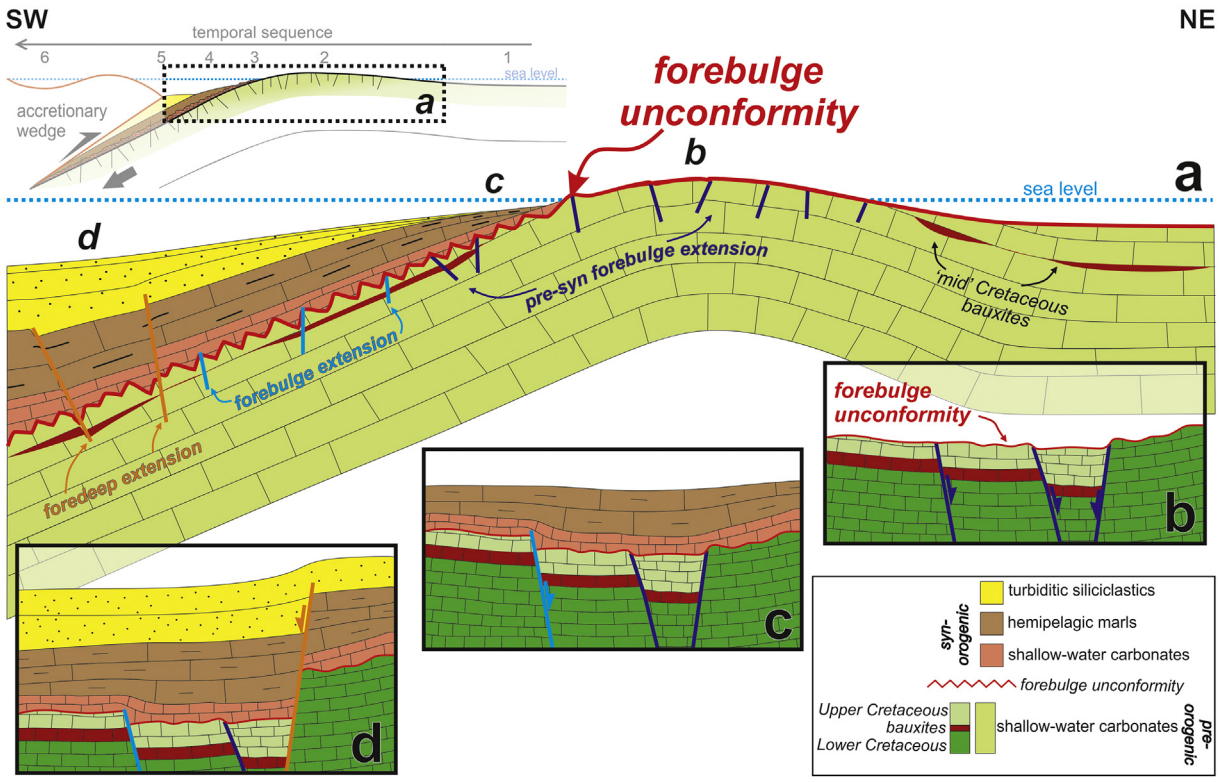


**Fig. 9.** Sketch showing the tectono-stratigraphic evolution of the foreland basin system at a regional scale (a) with details evidencing how, on a more local scale (b), the articulated topography created before/during the onset of foreland basin subsidence influences the syn-orogenic stratigraphic record from the shallow-water, hemipelagic (c), to siliciclastics turbiditic (d) deposition.

preserved above the unconformity track the time when the sea bottom subsided below the fair-weather wave base. They give, hence, the age of the base of the forebulge depozone, which is a significant point in the evolution of the foreland basin.

### 5.1. Age constraints

The age of the base of the lower Miocene limestones of the Matese Mts was previously poorly constrained. A Burdigalian age was proposed, based on the presence of the bivalve *Pecten pseudobeudanti* (Carannante and Simone, 1996). More to the north, at Mt. Cairo, in the Aurunci Mts, *Miogypsina globulina* (Michelotti) has been found at the base of the Calcari a Briozoi e Litotamni Fm. (Brandano et al., 2007), which represents the equivalent of the Cusano Fm. in the central Apennines. The same species is also reported in the lower Miocene limestones of the Roccadaspide Fm. at Capaccio (Cilento promontory; unpublished data cited in Brandano et al., 2007). *Miogypsina globulina* is a marker for the lower part of the Shallow Benthic Zone 25 of Cahuzac and Poignant (1997). This larger foraminiferal biozone is considered to span the entire Burdigalian (Cahuzac and Poignant, 1997; Hilgen et al., 2012), which is characterized, in the Mediterranean realm, by the sequence of chronospecies *M. globulina*, *M. intermedia*, *M. cushmani* and *M. mediterranea* (Drooger, 1993, and references therein). Based on its evolutionary stage, the *M. globulina* population of the Mt. Cairo section, was considered indicative of the middle part of the lower Burdigalian (Brandano et al., 2007, pp. 226). However, it must be stressed that the chronostratigraphic calibration of the ranges of different chronospecies and, even more, of the different evolutionary stages of the same chronospecies, is very poorly constrained. For this reason, SIS offers a much more precise and reliable tool for high-resolution dating and correlation of lower Miocene shallow-water carbonates. The ages of 18.7–18.6 Ma for the base of the Cusano Fm. in the Matese Mts (Pietraroja and Regia Piana) fall within the middle portion of the Burdigalian, according to the GTS2012. Moreover, these ages, considering their error band, are within error from the age of 18.8 Ma obtained with SIS for the base of the Calcari a Briozoi and Litotamni Fm. in the Mt. Lungo section (Aurunci Mts, central Apennines) by Brandano and Policicchio (2012).

A considerably younger age, 16.3 Ma, is given by SIS for the base of the Cusano Fm. in the Mt. Camposauro area. A younger age for the base of the Miocene transgressive deposits overlying the forebulge unconformity at Mt. Camposauro, is consistent with the occurrence in this locality of a rather advanced population of *Miogypsina intermedia* (Schiavinotto, 1985). The SIS age obtained for the base of the syn-orogenic sequence at Mt. Camposauro would correspond to the uppermost part of the SBZ 25 and would extend the range of *M. intermedia* almost to the end of the Burdigalian. To this regard, it is worth mentioning that the range of *M. intermedia* is considered to extend into the N7 planktic foraminiferal zone (De Mulder, 1975), which corresponds to the upper part of the Burdigalian (Hilgen et al., 2012).

A precise reconstruction of the timing of the Miocene transgression over the whole central and southern Apennines, recorded by the base of the first shallow-water carbonates overlying the forebulge unconformity, is at the moment hindered by the absence of precisely constrained ages. In any case, this task is definitely beyond the resolution attainable with biostratigraphy. The available data indicate that from the Pollino massif in northern Calabria to the Aurunci Mts in Lazio, the first transgressive deposits contain *Miogypsina globulina* (Selli, 1957; Brandano et al., 2007). Specimens of the older *Miogypsina socini* were found only in few localities of the Cilento area (Fig. 10) (Carannante et al., 1988a; Carannante and Simone, 1996). The range of *M. socini* is referable to the middle-upper Aquitanian, while the range of *M. globulina*, most probably extending over a time interval of some million years, is at present considered to start at the Aquitanian-Burdigalian boundary (Cahuzac and Poignant, 1997; Hilgen et al., 2012). However, their calibration to the geological time scale is very poorly constrained. A much better resolution can at present only be pursued by SIS (Fig. 10).

### 5.2. The forebulge unconformity

The occurrence of the Miocene Apennine forebulge is testified by a regional unconformity separating the passive margin megasequence from syn-orogenic sediments (Figs. 1, 9) (Crampton and Allen, 1995). In the study area, the mid-upper Burdigalian syn-orogenic deposits lie on a passive margin paleosubstrate, which is Lower to Upper Cretaceous in age (Fig. 9, the "mid-Cretaceous" bauxites represent a guide level separating Lower from Upper Cretaceous limestones). Few and scattered localities witness also the deposition of Paleogene shallow-water carbonates (Selli, 1962; Chiocchini et al., 1994). Overall, from the southern to central Apennines, the age of the first syn-orogenic deposits overlying the unconformity ranges from early to late Miocene (Selli, 1957; Carannante et al., 1988a; Patacca et al., 2008; Carnevale et al., 2011; Brandano and Policicchio, 2012). A different interpretation is presented by Carminati et al. (2007), who proposed that the first interval of Miocene shallow-water carbonates was deposited during a phase of moderate uplift or stability related to the development of protothrusts or to foreland propagation of compressive stresses. The development of the forebulge unconformity and depozone shows differences in function of the environmental setting (Crampton and Allen, 1995). The latter is in turn related to geodynamics (e.g., flexural rigidity of the foreland lithosphere; Watts, 2001; DeCelles, 2012) and eustatism (Giles and Dickinson, 1995). Generally, in submarine deep-water settings, the stratigraphic record of the bulging and of the onset of flexural subsidence has a good potential of preservation, such as in the Aruma Group on the Wasia-Aruma Break unconformity in Oman and UAE (Robertson, 1987; Boote et al., 1990; Robertson and Searle, 1990; Ali and Watts, 2009; Cooper et al., 2014), the Gurpi-Pabdeh Group in Zagros (Alavi, 2004; Vergés et al., 2011; Saura et al., 2015), and in the Pinecone Sequence in Antler foreland of Nevada-Utah (Giles and Dickinson, 1995). In the Apennines, the peripheral bulge developed in subaerial conditions. The system thus evolved from subaerial to shallow-water, with generally incomplete preservation of the stratigraphic record. The facies transition from pre-, syn-, and post-bulging is only sporadically fully recorded in the Apennines, such as in the Cilento area of southern Apennines (Boni, 1974; Carannante et al., 1988a; Bianca et al., 2009; Monti et al., 2014) and in Scontrone and Palena areas of the central Apennines (Patacca et al., 2008; Carnevale et al., 2011). In most parts of the central-southern Apennines, including the study area, a paraconformity/disconformity (Bassi et al., 2010; Brandano, 2017) (Figs. 4a–c, 5a, 6a) is the only record left by the passage of the forebulge. This can be explained considering that, when sedimentation resumes in shallow-water environment (Fig. 9c), the marine transgression can be accompanied by erosion – i.e. ravinement – and sediment bypass, which can smooth the unconformity and remove the continental deposits of the subaerial phase and the transitional marine deposits of the first phase of the transgression (e.g., White et al., 2002; Babić and Zupanič, 2012; Brandano, 2017).

### 5.3. Local effects on a regional framework

In the study area, compared to the general regional configuration (Fig. 9a), the local topography of the top of the pre-orogenic sequence - Lower to Upper Cretaceous in age - appears more articulated. This influenced the development of the unconformity and the onset of syn-orogenic sedimentation (Fig. 9b). Accordingly, the diachrony between the first deposits of the Cusano Fm. at the Matese and Camposauro sites is likely related to such articulated topography. Prior to becoming the paleosubstrate of the

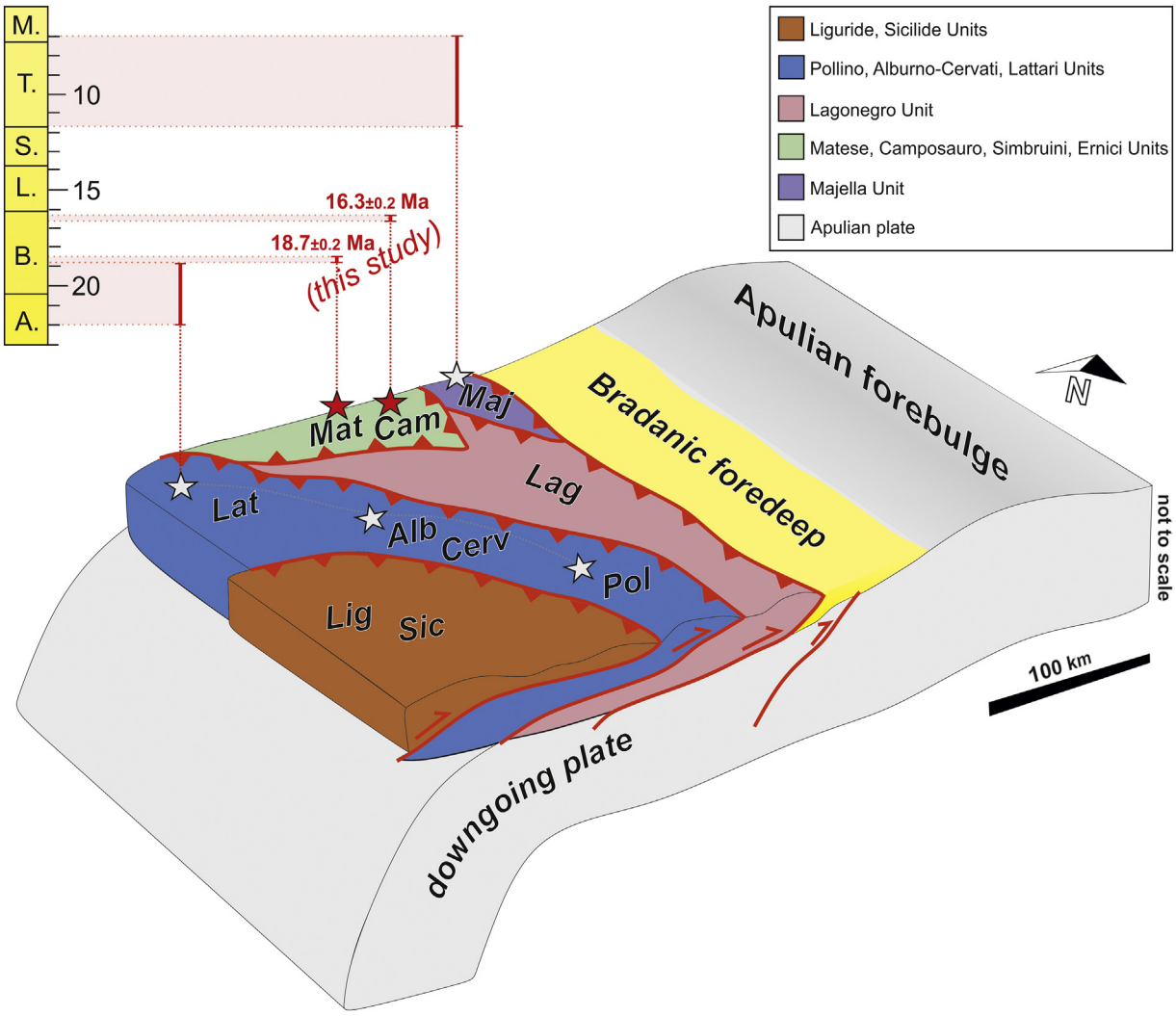


**Fig. 10.** Schematic reconstruction of the central-southern Apennines fold and thrust belt and of their foreland in the present-day configuration. The figure shows the age of the first syn-orogenic shallow-water carbonates at different locations within the Apennine orogenic belt. Biostratigraphic ages (white stars) are from the literature (Selli, 1957; De Blasio et al., 1981; Carannante et al., 1988b; Patacca et al., 2008). The strontium isotope ages for the Matese and Camposauro (red stars) are from the present study.

foreland basin, the top of the passive margin sequence formed a locally articulated and tectonically controlled paleotopography, as documented in the present Apulian forebulge (Doglioni et al., 1994; Mariotti and Doglioni, 2000; Billi and Salvini, 2003) and in the Hyblean Plateau (Billi et al., 2006). In particular, horst and graben structures were inherited by previous tectonic events (see the blue colored faults in Fig. 9b) (e.g., Calabrò et al., 2003; Vitale et al., 2018) and subsequently reactivated during the forebulge stage (e.g., Tavani et al., 2015b) (see the pale blue colored faults in Fig. 9c). In support of this reactivation, we also present data on meso-structures affecting the sedimentary rocks below and above the forebulge unconformity. Joints and veins in the Cretaceous and Miocene sedimentary rocks display similar orientations, i.e. bedding-perpendicular and striking mostly NNW-SSE to N-S and WSW-ENE to E-W, which are identical to the orientation of sedimentary dykes filled with Miocene sediments. This feature indicates a Miocene age for these extensional structures. Studies on the early-orogenic fracture patterns of the Apennines recognize similar trends both in the fold and thrust belt (e.g., Vitale et al., 2012; Carminati et al., 2014; Tavani et al., 2015b; Corradetti et al., 2018; La Bruna et al., 2018) and in the present-day forebulge (Billi and Salvini, 2003). In agreement with our interpretation, these studies have attributed the development of these extensional structures to the flexing of the lithosphere during the development of the forebulge. The ongoing flexure-related extension carried on with the acceleration of the subsidence (Carminati et al., 2007) and led to the drowning of the platform below the photic zone in the early Serravallian (Fig. 9c) (i.e., hemipelagic marls deposition of the Longano Fm., Lirer et al., 2005). Progressively, the system became involved in the foredeep setting (Pietraroja Fm., middle Tortonian; Selli, 1957; Lirer et al., 2005), where further structures were reactivated and formed (see the orange colored faults in Fig. 9d) (Tavani et al., 2015b). At this stage, the syn-orogenic sedimentation definitively switched into siliciclastic deposition (Fig. 9d).

The effect of eustatic sea-level changes on the first stages of the Miocene transgression in the southern Apennines should also be taken into account for a complete tectono-stratigraphic reconstruction. In this regard, Crampton and Allen (1995) stressed the role of long-term sea-level changes (i.e., second-order cycles of Haq et al., 1988) on the development of the forebulge unconformity. These long-term sea-level changes, lasting a similar amount of time to the duration of forebulge uplift, can have a greater impact than rapid oscillations. In our case, the onset of syn-orogenic sedimentation at

the Matese and Camposauro sites occurred during a global (2nd order) sea-level lowstand (Haq et al., 1988; Brandano and Corda, 2002; Brandano and Policicchio, 2012), which further emphasizes the role of tectonic subsidence in driving the transgression. On the other hand, the age of the first syn-orogenic sediments at Camposauro can also reflect the influence of the higher-order sea-level rise in the latest Burdigalian (John et al., 2011; Kominz et al., 2016). Currently, the sedimentary record of the Miocene foreland of the central-southern Apennine belt is exposed in patches in different localities of the central-southern Apennines belt (Fig. 10) and this further complicates reconstructing the complete tectono-stratigraphic evolution of the foreland basin. Precise dating of the very first syn-orogenic deposits has been obtained through SIS only for some areas of the central Apennines (Brandano and Corda, 2002; Brandano and Policicchio, 2012) and for the Matese and Camposauro (this study). For other areas, only biostratigraphic ages are available, which are inadequate to constrain the evolution and migration of the foreland basin and orogenic belt system. In Fig. 10, the example of the poor resolution attained by biostratigraphy versus high resolution attained by SIS is illustrated considering the ages of Cerchiara, Roccadaspide and Recommone Fms (Selli, 1957; De Blasio et al., 1981; Carannante et al., 1988a), Cusano Fm. (this study) for the southern Apennines, and Lithothamnium Limestone Fm. (Tortonian – lower Messinian, Patacca et al., 2008) for the central Apennines.

## 6. Conclusions

The Miocene Apennine foreland basin system developed in a collisional-retreating setting, in which local and regional factors played a role in the development and configuration of forebulge unconformity and first syn-orogenic transgression. The ages of the first shallow-water carbonates overlying the forebulge unconformity provide a prime constraint to unravel the evolution of the Miocene foreland basin of the southern Apennine fold and thrust belt. Precise dating and correlation of these deposits by strontium isotope stratigraphy reveal a strongly diachronous timing of the onset of the syn-orogenic sedimentary sequence between the Matese Mts (18.7–18.6 Ma) and the Mt. Camposauro area (16.3 Ma), in the northern sector of the southern Apennines. We discussed the possible reasons for the observed diachrony and finally identified that it can be explained as a smaller-scale local complication of inherited topography along with forebulge extension in the framework of a regional foreland basin system.

We observed and discussed that the development of the forebulge unconformity was accompanied by extensional deformation. Joints, veins, and sedimentary dykes developed during this stage pointing to an extensional regime. This indicates the flexing of the lithosphere during the forebulge stage.

We finally conclude that by extending the same approach of this work to other sectors of the southern Apennines, we could define for the first time the timing of deformation, and thus better constrain the amount and rate of shortening and trench retreat in the Apennine fold and thrust belt. Ultimately, the workflow used in this study could be applied to other fold and thrust belts where subaerial exposure has produced an incomplete record of the transition from bulging to foredeep.

## Declaration of competing interest

The authors declare that they have no known competing financial interests or personal relationships that could have appeared to influence the work reported in this paper.

## Acknowledgements

This research has been funded by the University of Naples Federico II (grant "Progetto di Ricerca di Ateneo" E62F17000190005 to MP). MS acknowledges financial support from the Ruth and Robert Weimer Fund, the John Sanders Fund, and the Friedman Student Research Fund (SEPM Foundation Student Research Grant). We thank Sylvia Riechelmann, Dieter Buhl and Kathrin Krimmler for the geochemical analyses at the Institut für Geologie, Mineralogie und Geophysik of the Ruhr-Universität of Bochum. We are grateful to Federico Lugli for his support and help with samples preparation and geochemical analyses at the University of Modena and Reggio Emilia. The editor Catherine Chagué and the reviewers Marco Brandano and José I. Cuitiño are greatly acknowledged for their review and constructive comments which improved the manuscript.

## References

Alavi, M., 2004. Regional stratigraphy of the Zagros fold-thrust belt of Iran and its proforeland evolution. Am. J. Sci. 304, 1–20.
Ali, M.Y., Watts, A.B., 2009. Subsidence history, gravity anomalies and flexure of the United Arab Emirates (UAE) foreland basin. GeoArabia 14, 17–44.
Allen, P.A., Homewood, P., Williams, G.D., 1986. Foreland basins: an introduction. In: Allen, P.A., Homewood, P. (Eds.), Foreland Basins. International Association of Sedimentology, pp. 3–12 Special Publication.
Ascione, A., Ciarcia, S., Di Donato, V., Mazzoli, S., Vitale, S., 2012. The Pliocene-Quaternary wedge-top basins of southern Italy: an expression of propagating lateral slab tear beneath the Apennines. Basin Res. 24, 456–474.
Babić, L., Zupanič, J., 2008. Evolution of a river-fed foreland basin fill: the North Dalmatian flysch revisited (Eocene, Outer Dinarides). Natura Croatica 17, 357–374.
Babić, L., Zupanič, J., 2012. Laterally variable development of a basin-wide transgressive unit of the North Dalmatian Foreland Basin (Eocene, Dinarides, Croatia). Geologia Croatica 65, 1–28.
Baruffini, L., Lottaroli, L., Torricelli, S., Lazzari, D., 2000. Stratigraphic revision of the Eocene Albidona Formation in the type locality (Calabria, Southern Italy). Rivista Italiana Di Paleontologia e Stratigrafia (Research In Paleontology and Stratigraphy) 106, 73–98.
Bassi, D., Carannante, G., Checconi, A., Simone, L., Vigorito, M., 2010. Sedimentological and palaeoecological integrated analysis of a Miocene channelized carbonate margin, Matese Mountains, Southern Apennines, Italy. Sediment. Geol. 230, 105–122.
Bernoulli, D., 2001. Mesozoic-Tertiary carbonate platforms, slopes and basins of the external Apennines and Sicily. In: Vai, G.B., Martini, I.P. (Eds.), Anatomy of an Orogen: The Apennines and Adjacent Mediterranean Basins. Springer, Dordrecht, pp. 307–325.
Bianca, M., Festa, A., Mammino, P., Monaco, C., 2009. Geological Map of Italy, Scale 1: 50000, Sheet 535 (Trebisacce). ISPRA, Rome.
Bigi, S., Milli, S., Corrado, S., Casero, P., Aldega, L., Botti, F., Moscatelli, M., Stanzione, O., Falcini, F., Marini, M., Cannata, D., 2009. Stratigraphy, structural setting and burial history of the Messinian Laga basin in the context of Apennine foreland basin system. Journal of Mediterranean Earth Sciences 1, 61–84.
Billi, A., Salvini, F., 2003. Development of systematic joints in response to flexure-related fibre stress in flexed foreland plates: the Apulian forebulge case history, Italy. J. Geodyn. 36, 523–536.
Billi, A., Porreca, M., Faccenna, C., Mattei, M., 2006. Magnetic and structural constraints for the noncylindrical evolution of a continental forebulge (Hyblea, Italy). Tectonics 25, 1–15.
Bonardi, G., Perrone, V., Ciampo, G., 1985. La Formazione di Albidona nell'Appennino calabro-lucano: ulteriori dati stratigrafici e relazioni con le unità esterne appenniniche. Boll. Soc. Geol. Ital. 104, 539–549 (in Italian, with English abstract).
Boni, M., 1974. Le argille rosse continentali del passaggio Paleocene-Miocene nella piattaforma carbonatica campano-lucana. Bollettino Della Società Geologica Italiana 93, 1059–1094 (in Italian, with English abstract).
Boote, D.R.D., Mou, D., Waite, R.I., 1990. Structural evolution of the Suneinah Foreland, Central Oman Mountains. Geol. Soc. Spec. Publ. 49, 397–418.
Bosellini, A., 2004. The western passive margin of Adria and its carbonate platforms. Special Volume of the Italian Geological Society for the 32nd International Geological Congress, Florence, Italy, pp. 79–92.
Bosence, D., 2005. A genetic classification of carbonate platforms based on their basinal and tectonic settings in the Cenozoic. Sediment. Geol. 175, 49–72.
Bradley, D.C., Kidd, W.S.F., 1991. Flexural extension of the upper continental crust in collisional foredeeps. Geol. Soc. Am. Bull. 103, 1416–1438.
Brandano, M., 2017. Unravelling the origin of a Paleogene unconformity in the Latium-Abruzzi carbonate succession: a shaved platform. Palaeogeogr. Palaeoclimatol. Palaeoecol. 485, 687–696.
Brandano, M., Corda, L., 2002. Nutrients, sea level and tectonics: constrains for the facies architecture of a Miocene carbonate ramp in central Italy. Terra Nova 14, 257–262.
Brandano, M., Policicchio, G., 2012. Strontium stratigraphy of the Burdigalian transgression in the Western Mediterranean. Lethaia 45, 315–328.
Brandano, M., Giannini, E., Schiavinotto, F., Verrubbi, V., 2007. Miogypsina globulina (Michelotti) from Lower Miocene Villa S. Lucia section (M. te Cairo, Central Apennines). Geol. Romana 40, 119–127.
Brandano, M., Corda, L., Castorina, F., 2010. Facies and sequence architecture of a tropical foramol-rhodalgal carbonate ramp: Miocene of the Central Apennines (Italy). In:

Mutti, M., Piller, W., Betzler, C. (Eds.), Carbonate Systems During the Oligocene-Miocene Climatic Transition: IAS (International Association of Sedimentologists) Special Publication. Wiley-Blackwell, Oxford, UK, pp. 107–128.
Cahuzac, B., Poignant, A., 1997. An attempt of biozonation of the Oligo-Miocene in the European basins, by means of larger neritic foraminifera. Bulletin de la Société géologique de France 168, 155–169.
Calabrò, R.A., Corrado, S., Di Bucci, D., Robustini, P., Tornaghi, M., 2003. Thin-skinned vs. thick-skinned tectonics in the Matese Massif, Central-Southern Apennines (Italy). Tectonophysics 377, 269–297.
Carannante, G., Simone, L., 1996. Rhodolith facies in the central-southern Apennines Mountains, Italy. In: Franseen, E.K., Esteban, M., Rouchy, J.M. (Eds.), Models for Carbonate Stratigraphy From Miocene Reef Complexes of Mediterranean Regions. Concepts in Sedimentology and Paleontology 5. Society of Economic Paleontologists and Mineralogists, pp. 261–275.
Carannante, G., Matarazzo, R., Pappone, G., Severi, C., Simone, L., 1988a. Le calcareniti mioceniche della Formazione di Roccadaspide (Appennino campano-lucano). Mem. Soc. Geol. Ital. 41, 775–789 (in Italian, with English abstract).
Carannante, G., Esteban, M., Milliman, J.D., Simone, L., 1988b. Carbonate lithofacies as paleolatitude indicators: problems and limitations. Sediment. Geol. 60, 333–346.
Carannante, G., Cesarano, M., Pappone, G., Putignano, M.L., 2013. Illustrative Notes of the Geological Map of Italy, Scale 1:50000, Sheet 431 (Caserta Est). ISPRA, Rome.
Carminati, E., Corda, L., Mariotti, G., Brandano, M., 2007. Tectonic control on the architecture of a Miocene carbonate ramp in the Central Apennines (Italy): insights from facies and backstripping analyses. Sediment. Geol. 198, 233–253.
Carminati, E., Fabbi, S., Santantonio, M., 2014. Slab bending, syn-subduction normal faulting, and out-of-sequence thrusting in the Central Apennines. Tectonics 33, 530–551.
Carnevale, G., Patacca, E., Scandone, P., Pisa, U., 2011. Field guide to the post-conference excursions (Scontrone, Palena and Montagna della Majella). International Conference "Neogene Park: Vertebrate Migration in the Mediterranean & Paratethys". Regional Committee on Mediterranean Neogene Stratigraphy Interim Colloquium, Scontrone (L'Aquila), Italy, pp. 1–98.
Cello, G., Mazzoli, S., 1998. Apennine tectonics in southern Italy: a review. J. Geodyn. 27, 191–211.
Chiocchini, M., Farinacci, A., Mancinelli, A., Molinari, V., Potetti, M., 1994. Biostratigrafia a foraminiferi, dasicladali e calpionelle delle successioni carbonatiche mesozoiche dell'Appennino centrale (Italia). In: Mancinelli, A. (Ed.), Biostratigrafia dell'Italia Centrale. Studi Geologici Camerti, pp. 9–129 (in Italian, with English abstract).
Cipollari, P., Cosentino, D., 1995. Miocene unconformities in the Central Apennines: geodynamic significance and sedimentary basin evolution. Tectonophysics 252, 375–389.
Civitelli, G., Brandano, M., 2005. The «Calcari a Briozoi e Litotamni» in the Latium-Abruzzi carbonate platform (Central Apennines, Italy): atlas of the lithofacies and depositional model. Bollettino Della Società Geologica Italiana 124, 611–643.
Cooper, D.J.W.W., Ali, M.Y., Searle, M.P., 2014. Structure of the northern Oman Mountains from the Semail Ophiolite to the Foreland Basin. Geol. Soc. Lond., Spec. Publ. 392, 129–153.
Corradetti, A., Tavani, S., Parente, M., Iannace, A., Vinci, F., Pirmez, C., Torrieri, S., Giorgioni, M., Pignalosa, A., Mazzoli, S., 2018. Distribution and arrest of vertical through-going joints in a seismic-scale carbonate platform exposure (Sorrento peninsula, Italy): insights from integrating field survey and digital outcrop model. J. Struct. Geol. 108, 121–136.
Corradetti, A., Spina, V., Tavani, S., Ringenbach, J.C., Sabbatino, M., Razin, P., Laurent, O., Brichau, S., Mazzoli, S., 2019. Late-stage tectonic evolution of the Al Hajar Mountains, Oman: new constraints from Paleogene sedimentary units and low-temperature thermochronometry. Geol. Mag., 1–14 https://doi.org/10.1017/S0016756819001250.
Cosentino, D., Cipollari, P., Marsili, P., Scrocca, D., 2010. Geology of the central Apennines: a regional review. J. Virtual Explor. 36, 1–37.
Crampton, S.L., Allen, P.A., 1995. Recognition of forebulge unconformities associated with early stage foreland basin development: example from the North Alpine Foreland Basin. AAPG Bull. 79, 1495–1514.
Critelli, S., Muto, F., Tripodi, V., Perri, F., Schattner, U., 2011. Relationships between lithospheric flexure, thrust tectonics and stratigraphic sequences in foreland setting: the Southern Apennines foreland basin system, Italy. Tectonics 2, 121–170.
De Blasio, I., Lima, A., Perrone, V., Russo, M., 1981. Nuove vedute sui depositi miocenici della Penisola Sorrentina. Bollettino Della Società Geologica Italiana 100, 57–70 (in Italian, with English abstract).
De Capoa, P., Di Donato, V., Di Staso, A., Giardino, S., Rinaldi, S., 2003. Preparation techniques and methodological approach to calcareous nannoplankton analysis in silico-and calciclastic turbidites. Courier-Forschungsinstitut Senckenberg 244, 105–128.
De Mulder, E.F.J., 1975. Microfauna and Sedimentary-Tectonic History of the Oligo-Miocene of the Ionian Islands and Western Epirus (Greece). PhD Thesis. Utrecht University, Utrecht, Netherlands.
DeCelles, P.G., 2012. Foreland basin systems revisited: variations in response to tectonic settings. In: Busby, C., Azor, Pérez A. (Eds.), Tectonics of Sedimentary Basins: Recent Advances. Blackwell Publishing Ltd., Chichester, UK, pp. 405–426.
DeCelles, P.G., Giles, K.A., 1996. Foreland basin systems. Basin Res. 8, 105–123.
DeCelles, P.G., Gehrels, G.E., Quade, J., Ojha, T.P., 1998. Eocene-early Miocene foreland basin development and the history of Himalayan thrusting, western and central Nepal. Tectonics 17, 741–765.
DePaolo, D.J., Ingram, B., 1985. High-resolution stratigraphy with strontium isotopes. Science 227, 938–941.
Dewey, J.F., Helman, M.L., Knott, S.D., Turco, E., Hutton, D.H.W., 1989. Kinematics of the western Mediterranean. Geol. Soc. London, Spec. Publ. 45, 265–283.
Doglioni, C., 1991. A proposal for the kinematic modelling of W-dipping subductions-possible applications to the Tyrrhenian-Apennines system. Terra Nova 3, 423–434.
Doglioni, C., 1995. Geological remarks on the relationships between extension and convergent geodynamic settings. Tectonophysics 252, 253–267.
Doglioni, C., Mongelli, F., Pieri, P., 1994. The Puglia uplift (SE Italy): an anomaly in the foreland of the Apenninic subduction due to buckling of a thick continental lithosphere. Tectonics 13, 1309–1321.
Dorobek, S.L., 1995. Synorogenic carbonate platforms and reefs in foreland basins: controls on stratigraphic evolution and platform/reef morphology. In: Dorobek, S.L., Ross, G.M. (Eds.), Stratigraphic Evolution of Foreland Basins. 52. SEPM (Society for Sedimentary Geology), pp. 127–147 Special Publication.
Drooger, C.W., 1993. Radial foraminifera; morphometrics and evolution. Verhandelingen der Koninklijke Nederlandse Akademie van Wetenschappen. Afdeling Natuurkunde. vol. 41, pp. 1–242.
Faccenna, C., Becker, T.W., Lucente, F.P., Jolivet, L., Rossetti, F., 2001. History of subduction and back-arc extension in the Central Mediterranean. Geophys. J. Int. 145, 809–820.
Faccenna, C., Becker, T.W., Auer, L., Billi, A., Boschi, L., Brun, J.P., Capitanio, F.A., Funiciello, F., Horvàth, F., Jolivet, L., Piromallo, C., Royden, L., Rossetti, F., Serpelloni, E., 2014. Mantle dynamics in the Mediterranean. Rev. Geophys. 52, 283–332.
Frijia, G., Parente, M., 2008. Strontium isotope stratigraphy in the upper Cenomanian shallow-water carbonates of the southern Apennines: short-term perturbations of marine 87Sr/86Sr during the oceanic anoxic event 2. Palaeogeogr. Palaeoclimatol. Palaeoecol. 261, 15–29.
Frijia, G., Parente, M., Di Lucia, M., Mutti, M., 2015. Carbon and strontium isotope stratigraphy of the Upper Cretaceous (Cenomanian-Campanian) shallow-water carbonates of southern Italy: chronostratigraphic calibration of larger foraminifera biostratigraphy. Cretac. Res. 53, 110–139.
Galewsky, J., 1998. The dynamics of foreland basin carbonate platforms: tectonic and eustatic controls. Basin Res. 10, 409–416.
Giles, K.A., Dickinson, W.R., 1995. The interplay of eustasy and lithospheric flexure in forming stratigraphic sequences in foreland settings: an example from the Antler foreland, Nevada and Utah. In: Dorobek, S.L., Ross, G.M. (Eds.), Stratigraphic Evolution of Foreland Basins. 52. SEPM (Society for Sedimentary Geology), pp. 187–211 Special Publication.
Glennie, K.W., Boeuf, M.G.A., Hughes Clarke, M.W., Moody-Stuart, M., Pilaar, W.F.H., Reinhardt, B.M., 1973. Late Cretaceous nappes in Oman Mountains and their geologic evolution. AAPG Bull. 58, 895–898.
Gradstein, F.M., Ogg, J.G., Schmitz, M., Ogg, G., 2012. The Geologic Time Scale 2012. Elsevier, Boston (1176 pp).
Haq, B.U., Hardenbol, J., Vail, P.R., 1988. Mesozoic and Cenozoic chronostratigraphy and cycles of sea level change. In: Wilgus, C.K., Hastings, B.S., Ross, C.A., Posamentier, H., Van Wagoner, J., Kendall, C.G.St.C. (Eds.), Sea Level Changes: An Integrated Approach. 42. SEPM (Society for Sedimentary Geology), pp. 71–108 Special Publication.
Hilgen, F.J., Lourens, L.J., Van Dam, J.A., Beu, A.G., Boyes, A.F., Cooper, R.A., Krijgsman, W., Ogg, J.G., Piller, W.E., Wilson, D.S., 2012. The Neogene period. In: Gradstein, F.M., Ogg, J.G., Schmitz, M., Ogg, G. (Eds.), The Geologic Time Scale 2012. Elsevier, Boston, pp. 923–978.
Iannace, A., Vitale, S., D'errico, M., Mazzoli, S., Di Staso, A., Macaione, E., Messina, A., Reddy, S.M., Somma, R., Zamparelli, V., 2007. The carbonate tectonic units of northern Calabria (Italy): a record of Apulian palaeomargin evolution and Miocene convergence, continental crust subduction, and exhumation of HP–LT rocks. J. Geol. Soc. 164, 1165–1186.
John, C.M., Karner, G.D., Browning, E., Leckie, R.M., Mateo, Z., Carson, B., Lowery, C., 2011. Timing and magnitude of Miocene eustasy derived from the mixed siliciclastic-carbonate stratigraphic record of the northeastern Australian margin. Earth Planet. Sci. Lett. 304, 455–467.
Kominz, M.A., Miller, K.G., Browning, J.V., Katz, M.E., Mountain, G.S., 2016. Miocene relative sea level on the New Jersey shallow continental shelf and coastal plain derived from one-dimensional backstripping: a case for both eustasy and epeirogeny. Geosphere 12, 1437–1456.
La Bruna, V., Agosta, F., Lamarche, J., Viseur, S., Prosser, G., 2018. Fault growth mechanisms and scaling properties in foreland basin system: the case study of Monte Alpi, Southern Apennines, Italy. J. Struct. Geol. 116, 94–113.
Lees, A., 1975. Possible influence of salinity and temperature on modern shelf carbonate sedimentation. Mar. Geol. 19, 159–198.
Leszczyński, S., Nemec, W., 2015. Dynamic stratigraphy of composite peripheral unconformity in a foredeep basin. Sedimentology 62, 645–680.
Lirer, F., Persico, D., Vigorito, M., 2005. Calcareous plankton biostratigraphy and age of the Middle Miocene deposits of Longano Formation (eastern Matese Mountains, southern Apennines). Riv. Ital. Paleontol. Stratigr. 111, 91–108.
Malinverno, A., Ryan, W.B.F., 1986. Extension in the Tyrrhenian Sea and shortening in the Apennines as result of arc migration driven by sinking of the lithosphere. Tectonics 5, 227–245.
Mariotti, G., Doglioni, C., 2000. The dip of the foreland monocline in the Alps and Apennines. Earth Planet. Sci. Lett. 181, 191–202.
Martinelli, M., Bistacchi, A., Balsamo, F., Meda, M., 2019. Late Oligocene to Pliocene extension in the Maltese Islands and implications for geodynamics of the Pantelleria Rift and Pelagian Platform. Tectonics 38, 3394–3415.
Mazzoli, S., Helman, M., 1994. Neogene patterns of relative plate motion for Africa-Europe: some implications for recent central Mediterranean tectonics. Geol. Rundsch. 83, 464–468.
McArthur, J.M., 1994. Recent trends in strontium isotope stratigraphy. Terra Nova 6, 331–358.
McArthur, J.M., Howarth, R.J., Bailey, T.R., 2001. Strontium isotope stratigraphy: LOWESS Version 3: best fit to the marine Sr-isotope curve for 0–509 Ma and accompanying look-up table for deriving numerical age. J. Geol. 109, 155–170.

McArthur, J.M., Howarth, R.J., Shields, G.A., 2012. Strontium isotope stratigraphy. In: Gradstein, F.M., Ogg, J.G., Schmitz, M.D., Ogg, G. (Eds.), The Geologic Time Scale 2012. Elsevier, Boston, pp. 127–144.

Mindszenty, A., D'Argenio, B., Aiello, G., 1995. Lithospheric bulges recorded by regional unconformities. The case of Mesozoic-Tertiary Apulia. Tectonophysics 252, 137–161.

Monti, L., Sgrosso, I., Graziano, R., Amore, F., Morabito, S., Santini, U., Vecchio, E., Castellano, M.C., D'Argenio, B., Marsella, E., Putignano, M.L., Conforti, A., De Vita, P., Fiano, V., Guida, D., Pescatore, E., Priore, A., Sgosso, A., Tescione, M., Aiello, G., Boudillon, F., De Lauro, M., De Martino, G., D'Isanto, C., Innangi, S., Marsella, E., Passaro, S., Pelosi, N., Ruggeri, S., Scotto di Vettimo, P., Tonielli, R., Capodanno, M., Molisso, F., Aiello, G., Ferraro, L., 2014. Geological Map of Italy, Scale 1:50000, Sheet 520 (Sapri). ISPRA, Rome.

Noguera, A.M., Rea, G., 2000. Deep structure of the Campanian–Lucanian arc (southern Apennine, Italy). Tectonophysics 324, 239–265.

Ogniben, L., 1958. Stratigrafia e microfaune del terziario della zona di Caiazzo (Caserta). Riv. Ital. Paleontol. Stratigr. 64, 199–286 (in Italian).

Ori, G.G., Roveri, M., Vannoni, F., 1986. Plio-Pleistocene sedimentation in the Apenninic-Adriatic foredeep (Central Adriatic Sea, Italy). In: Allen, P.A., Homewood, P. (Eds.), Foreland Basins. International Association of Sedimentologists, pp. 183–198 Special Publication.

Otoničar, B., 2007. Upper Cretaceous to Paleogene forbulge unconformity associated with foreland basin evolution (Kras, Matarsko Podolje and Istria; SW Slovenia and NW Croatia). Acta Carsologica 36, 101–120.

Patacca, E., Scandone, P., 2007. Geology of the southern Apennines. Bollettino Della Società Geologica Italiana 7, 75–119.

Patacca, E., Scandone, P., Mazza, P., 2008. The Miocene land-vertebrate fossil site of Scontrone (Central Apennines, Italy). Bollettino Della Società Geologica Italiana 127, 51–73.

Robertson, A.H.F., 1987. Upper Cretaceous Muti Formation: transition of a Mesozoic carbonate platform to a foreland basin in the Oman Mountains. Sedimentology 34, 1123–1142.

Robertson, A.H.F., Searle, M.P., 1990. The northern Oman Tethyan continental margin: stratigraphy, structure, concepts and controversies. Geol. Soc. Lond., Spec. Publ. 49, 3–25.

Roure, F., Casero, P., Vially, R., 1991. Growth processes and melange formation in the southern Apennines accretionary wedge. Earth Planet. Sci. Lett. 102, 395–412.

Saura, E., Garcia-Castellanos, D., Casciello, E., Parravano, V., Urruela, A., Vergés, J., 2015. Modeling the flexural evolution of the Amiran and Mesopotamian foreland basins of NW Zagros (Iran-Iraq). Tectonics 34, 377–395.

Scasso, R., McArthur, J., del Río, C., Martínez, S., Thirlwall, M., 2001. $^{87}Sr/^{86}Sr$ Late Miocene age of fossil molluscs in the 'Entrerriense' of the Valdés Peninsula (Chubut, Argentina). J. S. Am. Earth Sci. 14, 319–329.

Schiavinotto, F., 1979. Miogypsina e Lepidocyclina del Miocene di Monte La Serra (L'Aquila-Appennino centrale). Geol. Romana 18, 253–293 (in Italian).

Schiavinotto, F., 1985. Le Miogypsinidae alla base della trasgressione miocenica del Monte Camposauro (Appennino Meridionale). Bollettino Della Società Geologica Italiana 104, 53–63 (in Italian, with English abstract).

Selli, R., 1957. Sulla trasgressione del Miocene nell'Italia meridionale. Giorn. Geol. 26, 1–54 (in Italian).

Selli, R., 1962. Il Paleogene nel quadro della geologia dell'Italia Meridionale. Mem. Soc. Geol. Ital. 3, 733–789 (in Italian).

Sgrosso, I., 1998. Possibile evoluzione cinematica miocenica nell'orogene centro-sud-appenninico. Boll. Soc. Geol. Ital. 117, 679–724 (in Italian, with English abstract).

Simone, L., Carannante, G., Ruberti, D., Sirna, M., Sirna, G., Laviano, A., Tropeano, M., 2003. Development of rudist lithosomes in the Coniacian–Lower Campanian carbonate shelves of central-southern Italy: high-energy vs low-energy settings. Palaeogeogr. Palaeoclimatol. Palaeoecol. 200, 5–29.

Sinclair, H.D., 1997. Tectonostratigraphic model for underfilled peripheral foreland basins: an Alpine perspective. Geol. Soc. Am. Bull. 109, 324–346.

Steuber, T., 2003. Strontium isotope stratigraphy of Cretaceous hippuritid rudist bivalves: rates of morphological change and heterochronic evolution. Palaeogeogr. Palaeoclimatol. Palaeoecol. 200, 221–243.

Tavani, S., Storti, F., Lacombe, O., Corradetti, A., Muñoz, J.A., Mazzoli, S., 2015a. A review of deformation pattern templates in foreland basin systems and fold-and-thrust belts: implications for the state of stress in the frontal regions of thrust wedges. Earth Sci. Rev. 141, 82–104.

Tavani, S., Vignaroli, G., Parente, M., 2015b. Transverse versus longitudinal extension in the foredeep-peripheral bulge system: role of Cretaceous structural inheritances during early Miocene extensional faulting in inner central Apennines belt. Tectonics 34, 1412–1430.

Tavani, S., Corradetti, A., Sabbatino, M., Morsalnejad, D., Mazzoli, S., 2018. The Meso-Cenozoic fracture pattern of the Lurestan region, Iran: the role of rifting, convergence, and differential compaction in the development of pre-orogenic oblique fractures in the Zagros Belt. Tectonophysics 749, 104–119.

Turcotte, D.L., Schubert, G., 1982. Geodynamics. Wiley, New York (450 pp).

Ullmann, C.V., Korte, C., 2015. Diagenetic alteration in low-Mg calcite from macrofossils: a review. Geological Quarterly 59, 3–20.

Vergés, J., Marzo, M., Santaeulària, T., Serra-Kiel, J., Burbank, D.W., Muñoz, J.A., Giménez-Montsant, J., 1998. Quantified vertical motions and tectonic evolution of the SE Pyrenean foreland basin. Geol. Soc. Spec. Publ. 134, 107–134.

Vergés, J., Saura, E., Casciello, E., Fernàndez, M., Villaseñor, A., Jiménez-Munt, I., García-Castellanos, D., 2011. Crustal-scale cross-sections across the NW Zagros belt: implications for the Arabian margin reconstruction. Geol. Mag. 148, 739–761.

Vitale, S., Ciarcia, S., 2013. Tectono-stratigraphic and kinematic evolution of the southern Apennines/Calabria–Peloritani Terrane system (Italy). Tectonophysics 583, 164–182.

Vitale, S., Ciarcia, S., 2018. Tectono-stratigraphic setting of the Campania region (Southern Italy). Journal of Maps 14, 9–21.

Vitale, S., Dati, F., Mazzoli, S., Ciarcia, S., Guerriero, V., Iannace, A., 2012. Modes and timing of fracture network development in poly-deformed carbonate reservoir analogues, Mt. Chianello, southern Italy. J. Struct. Geol. 37, 223–235.

Vitale, S., Amore, O.F., Ciarcia, S., Fedele, L., Grifa, C., Prinzi, E.P., Tavani, S., Tramparulo, F.D., 2018. Structural, stratigraphic, and petrological clues for a Cretaceous–Paleogene abortive rift in the southern Adria domain (southern Apennines, Italy). Geol. J. 53, 660–681.

Vitale, S., Prinzi, E.P., Ciarcia, S., Sabbatino, M., Tramparulo, F.D.A., Verazzo, G., 2019. Polyphase out-of-sequence thrusting and occurrence of marble detritus within the wedge-top basin deposits in the Mt. Massico (southern Apennines): insights into the late Miocene tectonic evolution of the central Mediterranean. Int. J. Earth Sci. 108, 501–519.

Watts, A.B., 2001. Isostasy and Flexure of the Lithosphere. Cambridge University Press, Cambridge, UK (478 pp).

White, T., Furlong, K., Arthur, M., 2002. Forebulge migration in the Cretaceous Western interior basin of the Central United States. Basin Res. 14, 43–54.

Yu, H.S., Chou, Y.W., 2001. Characteristics and development of the flexural forebulge and basal unconformity of Western Taiwan Foreland Basin. Tectonophysics 333, 277–291.

Zamparelli, V., Cirilli, S., Iannace, A., Jadoul, F., 1999. Palaeotectonic and palaeoceanographic controls on microbial–serpulid communities in the Norian–Rhaetian carbonates of Italy: a synthesis. In: Colacicchi, R., Parisi, G., Zamparelli, V. (Eds.), Bioevents and Integrated Stratigraphy of the Triassic and the Jurassic in Italy. Paleopelagos, Special Publications 3, pp. 7–84.